CELLULAR NEUROSCIENCE

RNF220 is an E3 ubiquitin ligase for AMPA receptors to regulate synaptic transmission

Pengcheng Ma[1]†, Li Pear Wan[1,2]†, Yuwei Li[1,2]†, Chun-Hui He[3]†, Ning-Ning Song[4,5], Shiping Zhao[1], Huishan Wang[1,2], Yu-Qiang Ding[3,4,5]*, Bingyu Mao[1,6]*, Nengyin Sheng[1,6]*

Copyright © 2022 The Authors, some rights reserved; exclusive licensee American Association for the Advancement of Science. No claim to original U.S. Government Works. Distributed under a Creative Commons Attribution NonCommercial License 4.0 (CC BY-NC).

The accurate expression of postsynaptic AMPA receptors (AMPARs) is critical for information processing in the brain, and ubiquitination is a key regulator for this biological process. However, the roles of E3 ubiquitin ligases in the regulation of AMPARs are poorly understood. Here, we find that RNF220 directly interacts with AMPARs to meditate their polyubiquitination, and RNF220 knockout specifically increases AMPAR protein levels, thereby enhancing basal synaptic activity while impairing synaptic plasticity. Moreover, depending on its E3 ubiquitin ligase activity, RNF220 represses AMPAR-mediated excitatory synaptic responses and their neuronal surface expression. Furthermore, learning and memory are altered in forebrain RNF220-deficient mice. In addition, two neuropathology-related RNF220 variants fail to repress excitatory synaptic activity because of the incapability to regulate AMPAR ubiquitination due to their attenuated interaction. Together, we identify RNF220 as an E3 ubiquitin ligase for AMPARs and establish its substantial role in excitatory synaptic transmission and brain function.

INTRODUCTION

AMPA receptors (AMPARs) are ionotropic glutamatergic receptors that mediate fast excitatory synaptic neurotransmission in the brain, and their numbers on the postsynaptic membrane determine the strength and efficiency of basal synaptic activity. Synaptic plasticity, a cellular mechanism of learning and memory, is also primarily attributed to its activity-dependent recruitment and internalization at excitatory synapse (*1*–*3*). Dysregulation of AMPAR dynamic neuronal trafficking is considered as one critical reason for neuropsychiatric and neurodegenerative diseases (*4*, *5*). AMPARs are tetramers of GluA1-GluA4 subunits, and it has been established that their intracellular C-terminal domains play critical roles during AMPAR trafficking to and from synapses. Besides through subunit-specific protein interactors, the C-terminal domains undergo many post-translational modifications (PTMs) contributing to synaptic activity and plasticity regulation (*3*, *6*, *7*). Although the ubiquitin-proteasome system (UPS) is recognized for its regulation of postsynaptic protein stability and its participation in synaptic transmission (*8*–*11*), our knowledge about the molecular regulators for AMPAR ubiquitination is markedly less than the identified phosphorylation kinases and binding partners for AMPAR trafficking.

E3 ubiquitin ligase determines the specificity of substrate protein for recognition and ubiquitination, and the known E3 ligases fall into two families containing RING domain or HECT domain (*12*). Although the ubiquitination of AMPAR subunits GluA1 to GluA4 has been reported (*13*–*17*), only few specific E3 ubiquitin ligases have been reported (*9*, *18*). HECT-type Nedd4 is the first identified E3 ligase that is directly responsible for mammalian AMPAR ubiquitination and for regulating AMPAR endocytosis and synaptic transmission (*13*, *19*). Ubiquitination of GluA1 by E3 ligase Nedd4L is involved in spontaneous neuronal activity, and this impairment contributes to neuron hyperactivity and epilepsy (*20*). EphA4 is an Eph receptor involved in synaptic plasticity, and it is found that RING-type E3 ligase APC^{Cdh1} interacts with it, thereby regulating GluA1 ubiquitination and proteasomal degradation during synaptic homeostatic plasticity (*21*). In addition, Roche's laboratory (*22*) screened a subset of transmembrane RING-type E3 ubiquitin ligases and identified RNF167 as an E3 to regulate AMPAR ubiquitination in an activity-dependent manner as well as synaptic transmission. However, more efforts are needed to study the molecular mechanism underlying AMPAR ubiquitination and its biological significance for physiological and pathological processes.

RNF220 is a RING-type ubiquitin E3 ligase lacking a transmembrane domain, and it expresses broadly in the central nervous system during development (*23*). Our and other laboratory's studies have revealed that RNF220 plays critical roles in neural cell fate determination and neural tube patterning (*23*–*28*). We have also noted that RNF220 is expressed in postmitotic neurons and its expression is intensively high in the hippocampus of adult mouse (*23*, *29*, *30*), but its function at this stage and this region is still unknown. Moreover, RNF220 mutations (R363Q and R365Q) are recently reported to cause brain abnormalities (*31*), and note that several symptoms of the patients are related to dysfunction of synaptic activity, such as intellectual disability and seizure. However, it remains unclear about the RNF220 ubiquitination substrate in mature neurons and whether it is involved in synaptic regulation and related brain function.

In this study, with the RNF220 forebrain knockout (KO) mouse model, we found that the AMPAR-mediated synaptic transmission was enhanced and protein levels of GluA1 and GluA2 subunits were increased after RNF220 depletion. Neural behavioral analyses showed that RNF220-deficient mice had altered learning and memory abilities. Mechanistically, RNF220 directly interacted with GluA1 and GluA2 to mediate their polyubiquitination and protein stability,

[1]State Key Laboratory of Genetic Resources and Evolution, Kunming Institute of Zoology, Chinese Academy of Sciences, Kunming 650223, China. [2]Kunming College of Life Science, University of Chinese Academy of Sciences, Kunming 650223, China. [3]Key Laboratory of Arrhythmias, Ministry of Education of China, East Hospital, and Department of Anatomy and Neurobiology, Tongji University School of Medicine, Shanghai 200092, China. [4]State Key Laboratory of Medical Neurobiology and MOE Frontiers Center for Brain Science, Institutes of Brain Science, Fudan University, Shanghai 200032, China. [5]Department of Laboratory Animal Science, Fudan University, Shanghai 200032, China. [6]Center for Excellence in Animal Evolution and Genetics, Chinese Academy of Sciences, Kunming 650223, China
*Corresponding author. Email: shengnengyin@mail.kiz.ac.cn (N.S.); mao@mail.kiz.ac.cn (B.M.); dingyuqiang@vip.163.com (Y.-Q.D.).
†These authors contributed equally to this work.

and this ubiquitination-dependent regulation is involved in AMPAR synaptic and surface expression. Moreover, the neuropathological-associated mutations abolished RNF220's capability to regulate AMPAR ubiquitination and synaptic expression. Therefore, we provide compelling evidence that RNF220 is an E3 ubiquitin ligase for AMPARs to regulate synaptic transmission. This ubiquitination-dependent modulation is involved in brain physiological function, while its dysregulation might be related to neural disorders.

RESULTS

Basal excitatory synaptic transmission is increased in *RNF220* KO mice

To examine the function of RNF220 in brain, we crossed *RNF220*$^{fl/fl}$ mice with *Emx1-Cre* mice to knock out RNF220 expression in the cerebral cortex and hippocampus, starting from late embryonic stage (*32*). Both the mRNA (relative levels: P10, 0.25 ± 0.03; P20, 0.21 ± 0.01; P60, 0.15 ± 0.01; Fig. 1A) and protein (relative levels: P10, 0.18 ± 0.02; P20, 0.14 ± 0.01; P60, 0.09 ± 0.03; Fig. 1B) expression of RNF220 were significantly reduced in hippocampal and cortical (fig. S1, A and B) lysates of the postnatal conditional KO (cKO) mice (*Emx1-Cre;RNF220*$^{fl/fl}$) at the examined ages. The remaining RNF220 expression might be from other cell types without Emx1-Cre or inability of Emx1-Cre–mediated deletion of RNF220 in the brain. Immunostaining analyses showed the absence of RNF220 in the cortex and hippocampus in the cKO mice at postnatal day 21 (P21; Fig. 1, C and D). Moreover, the RNF220 depletion in forebrain cells did not significantly affect body weight and brain weight examined at P60 (fig. S1, C and D). To determine whether the lack of RNF220 affects brain morphology, we performed hematoxylin and eosin staining on coronal brain slices from the cKO mice and their littermate controls at P21. There were no apparent macroscopic defects in the *RNF220* cKO brain, and the cellular organization of the cortex and hippocampus was preserved (fig. S1, E and F). Together, all these data indicate that RNF220 depletion in forebrain has no obvious effect on brain development.

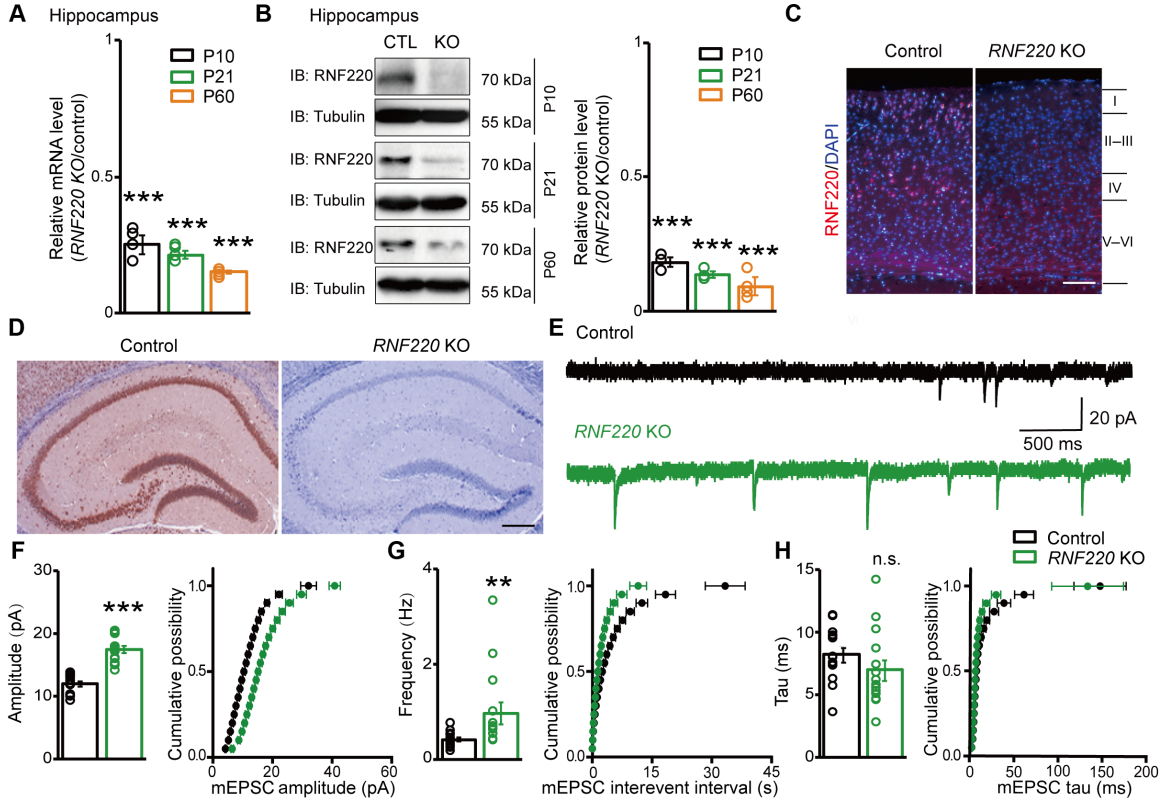

Fig. 1. Basal excitatory synaptic transmission is increased in *RNF220* KO mice. (**A** and **B**) mRNA (A) and protein (B) expression of RNF220 in hippocampus of *Emx1-Cre;RNF220*$^{fl/fl}$ mice and littermate controls (CTL) at P10, P21, and P60 ($n = 4$). (A) Real-time polymerase chain reaction (PCR) analyses of RNF220 mRNA levels using β-actin as the internal control. Bar graphs (mean ± SEM) show the relative mRNA expression normalized against respective littermate controls. Statistical analyses are compared to respective controls with unpaired *t* test. (B) Western blot analyses of RNF220 protein levels with α-tubulin as internal control. Bar graph (mean ± SEM) shows the relative expression normalized against respective littermate controls. Statistical analyses are compared to respective controls with unpaired *t* test. (**C** and **D**) Immunofluorescence and immunochemistry staining show the expression of RNF220 in cortical (C) and hippocampal (D) tissues, respectively, of *Emx1-Cre;RNF220*$^{fl/fl}$ mice and littermate controls at P21. Scale bars, 150 μm (C) and 300 μm (D). (**E**) Representative sample traces of CA1 pyramidal neuron mEPSCs from *Emx1-Cre;RNF220*$^{fl/fl}$ mice (green) and littermate controls (black) at P21. Scale bars, 20 pA/500 ms. (**F** to **H**) Analyses of mEPSC parameters from RNF220 KO ($n = 17$) and littermate control ($n = 14$) neurons. Bar graphs (mean ± SEM) show the amplitude (F), frequency (G), and decay kinetics (H). Statistical analyses are compared to respective controls with Mann-Whitney *U* test with Bonferroni correction. Cumulative distribution plots of mEPSC amplitude (F), frequency (G), and decay kinetics (H) from RNF220 KO (green) and control neurons (black). Cumulative distribution functions show no irregularities. IB, immunoblot; DAPI, 4′,6-diamidino-2-phenylindole. n.s. (not significant), $P > 0.05$; ***$P < 0.001$; and **$P < 0.01$.

Besides developmental delay, the patients harboring RNF220 mutations exhibit neuropsychiatric manifestations such as intellectual disability (*31*), which is closely related to dysregulation of synaptic transmission. We wondered whether the basal synaptic properties are affected after loss of RNF220. To this end, whole-cell patch-clamp recording was applied to examine the miniature excitatory postsynaptic currents (mEPSCs) of CA1 pyramidal neurons from acute hippocampal slices. We found that both the amplitude (control, 11.95 ± 0.56 pA; RNF220 KO, 17.45 ± 0.56 pA; Fig. 1F) and frequency (control, 0.42 ± 0.04 Hz; RNF220 KO, 0.96 ± 0.23 Hz; Fig. 1G) of AMPAR-mediated mEPSCs were significantly increased in *RNF220* cKO mice compared to the littermate controls, while there was no difference in the decay time (control, 8.2 ± 0.58 ms; RNF220 KO, 7 ± 0.82 ms; Fig. 1H). These results suggest that RNF220 is involved in the regulation of basal synaptic transmission.

RNF220 regulates synaptic activity by repressing AMPAR synaptic expression

As we have identified RNF220 as an E3 ubiquitin ligase regulating protein turnover in the central nervous system (*23*, *26*, *28*, *33*), it leads us to wonder whether the dysregulation of synaptic protein stability is the reason underlying the above phenotype. To this end, we used Western blot to examine the expression levels of critical synaptic proteins, especially the glutamate receptors, from RNF220-depleted hippocampus (Fig. 2A) and cerebral cortex (fig. S2A). It was found that in hippocampus homogenates, the protein levels of AMPAR subunits GluA1 and GluA2 (relative levels: GluA1, 2.99 ± 0.10; GluA2, 3.15 ± 0.15; Fig. 2B) were significantly and specifically increased in *RNF220* cKO mice, while there was no difference in *N*-methyl-D-aspartate receptor (NMDAR) subunit (relative levels: GluN1, 1.31 ± 0.14; GluN2A, 1.05 ± 0.04; GluN2B, 1.07 ± 0.05; Fig. 2B) expression compared to littermate controls, as well as postsynaptic PSD-95 (postsynaptic density protein 95; relative level: 1.00 ± 0.04; Fig. 2B) and presynaptic synaptophysin (relative level: 0.99 ± 0.07; Fig. 2B). Moreover, we found that in synaptosomal (relative levels: GluA1, 2.74 ± 0.22; GluA2, 2.88 ± 0.06; GluN1, 1.08 ± 0.07; GluN2A, 1.04 ± 0.05; GluN2B, 1.00 ± 0.06; PSD-95, 1.03 ± 0.04; synaptophysin, 0.99 ± 0.06; Fig. 2C) and postsynaptic density (relative levels: GluA1, 2.16 ± 0.21; GluA2, 2.89 ± 0.19; GluN1, 1.07 ± 0.06; GluN2A, 1.01 ± 0.05; GluN2B, 1.06 ± 0.05; PSD-95, 1.09 ± 0.06; Fig. 2D) fractions, the expression of GluA1 and GluA2 receptors, but not GluN1, GluN2A, GluN2B, PSD-95, or synaptophysin, was increased when RNF220 was deleted. Similar results were found in cerebral cortex tissue (fig. S2, A to D). Moreover, when mRNA levels of all these genes in the hippocampus and cortex were quantitatively examined by real-time polymerase chain reaction (PCR) experiments, there was no significant change (fig. S2E).

Given the above data suggesting that the protein levels of GluA1 and GluA2 receptors are regulated by RNF220, we next determined whether AMPAR-mediated synaptic transmission is affected when RNF220 is inactivated in neurons. To sparsely knock out *RNF220* in pyramidal neurons, Cre recombinase–expressed adeno-associated virus (AAV) was stereotactically injected into the hippocampal CA1 region of *RNF220*$^{fl/fl}$ mice on P0. Then, three weeks later, dual whole-cell recording was applied to test the evoked EPSCs (eEPSCs) from Cre/enhanced green fluorescent protein (EGFP) expressing and neighboring control pyramidal neurons simultaneously (Fig. 3A). It was found that AMPAR-mediated EPSCs were significantly higher in *RNF220* KO CA1 neurons compared to the respective neighboring controls (RNF220 KO, 190.48 ± 19.10% control; Fig. 3B), while the paired-pulse ratio was not significantly changed (control, 1.61 ± 0.20; RNF220 KO, 1.47 ± 0.21; Fig. 3C). Moreover, there was also no significant difference of paired-pulse ratio between the CA1 pyramidal neurons from *RNF220* cKO mice and control littermates (control, 1.80 ± 0.08; RNF220 KO, 2.02 ± 0.09; Fig. 3E). All these results suggest that the RNF220 loss enhances excitatory synaptic transmission by regulating the postsynaptic AMPAR expression but not the presynaptic release probability. We next examined the regulation of synaptic plasticity by RNF220 by inducing LTP (long-term potentiation) of the CA1 pyramidal neurons from *RNF220* cKO

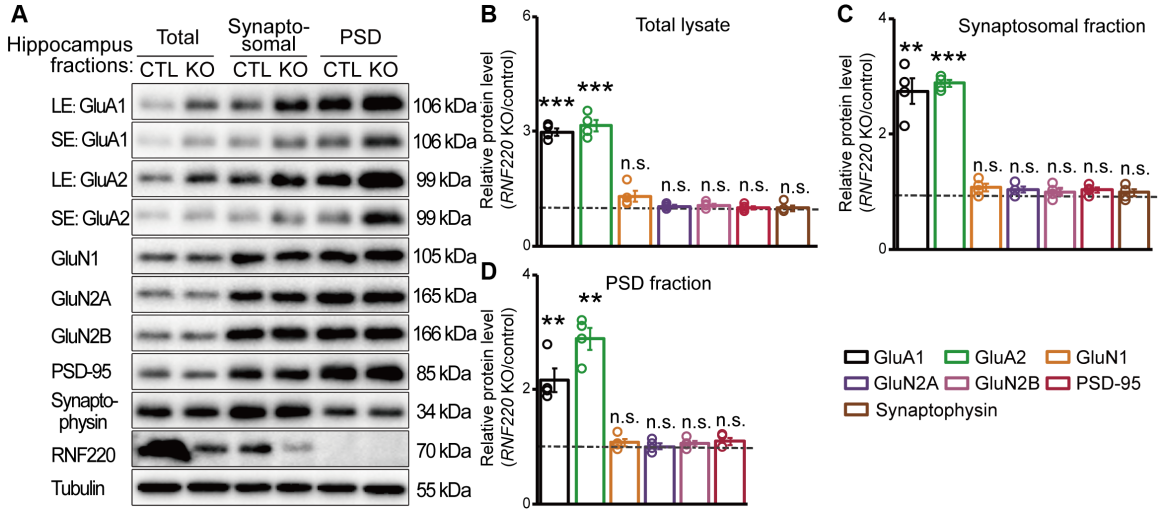

Fig. 2. RNF220 regulates synaptic and extrasynaptic AMPAR expression. (**A**) Western blot analyses of the expression levels of indicated synaptic proteins in the total lysates and synaptosomal and PSD fractions from hippocampus of *Emx1-Cre;RNF220*$^{fl/fl}$ mice ($n = 4$) and littermate controls ($n = 4$). α-Tubulin was used as the internal control. GluA1 and GluA2 expression levels with long and short exposure as indicated. (**B** to **D**) Bar graphs (mean ± SEM), overlaid with the actual data points, show the relative expression normalized against each respective littermate controls. Statistical analyses are compared to respective controls with unpaired *t* test. E, long exposure; SE, short exposure. n.s., $P > 0.05$; ***$P < 0.001$; and **$P < 0.01$.

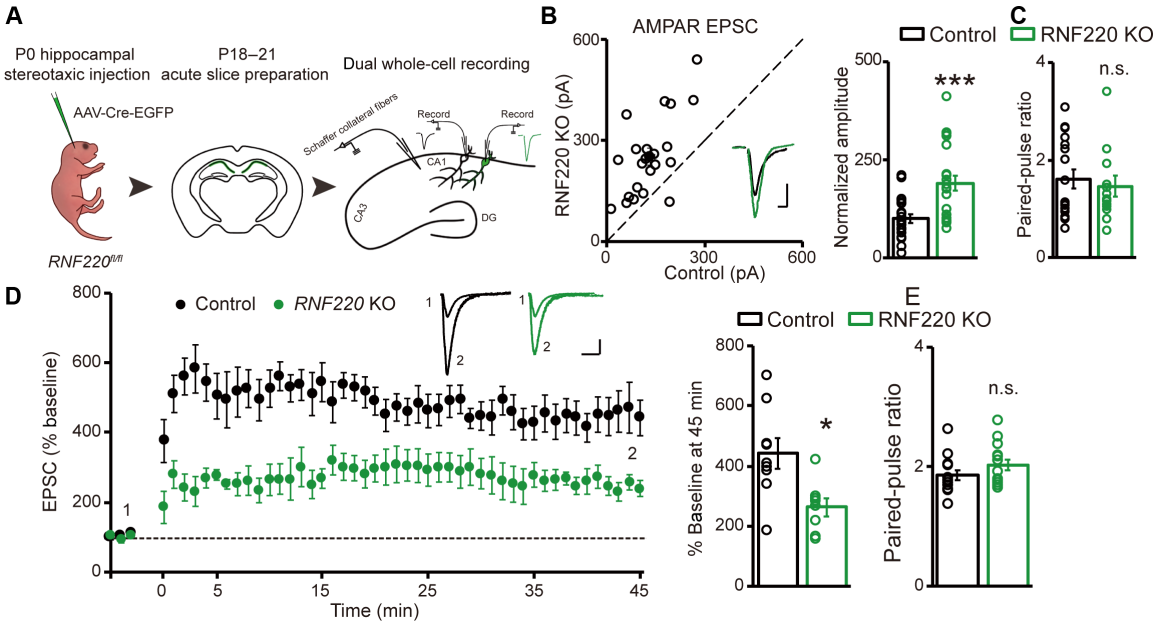

Fig. 3. RNF220 regulates excitatory synaptic transmission and plasticity. (**A**) Schematic cartoon of the experimental workflows on *RNF220*$^{fl/fl}$ mice. (**B** and **C**) Simultaneous recordings from a transfected CA1 pyramidal neuron (green trace) and a neighboring control one (black trace) were performed, and the eEPSCs were measured at −70 mV. (B) Open and filled circles represent amplitudes for single pairs and mean ± SEM, respectively. Insets show sample current traces from control (black) and experimental (green) cells. Scale bars, 100 pA/20 ms. Bar graphs (mean ± SEM, $n = 22$) show normalized eEPSC amplitudes presented in scatterplots. Statistical analyses are compared to controls with two-tailed Wilcoxon signed-rank sum test. (C) Paired-pulse ratios from control ($n = 17$) and KO ($n = 17$) neurons are shown in the bar graph (mean ± SEM) overlaid with the actual data points, and statistical analyses are compared to controls with Mann-Whitney *U* test with Bonferroni correction. (**D**) Whole-cell paired-LTP recordings were performed from CA1 pyramidal neurons of *Emx1-Cre;RNF220*$^{fl/fl}$ mice (green, $n = 8$) and littermate controls (black, $n = 9$), and the data are shown as the percentage of the respective baseline before LTP induction (mean ± SEM). The bar graph (mean ± SEM) shows normalized eEPSC amplitudes at 45 min after LTP induction. Sample traces show EPSCs before (*1*) and 45 min after LTP (*2*). Scale bars, 25 pA/25 ms. Statistical analyses are compared to controls with unpaired *t* test. (**E**) Paired-pulse ratios from *Emx1-Cre;RNF220*$^{fl/fl}$ mice ($n = 14$) and littermates ($n = 14$) are shown in the bar graph (mean ± SEM). Statistical analyses are compared to controls with Mann-Whitney *U* test with Bonferroni correction. n.s., $P > 0.05$; ***$P < 0.001$; and **$P < 0.01$.

mice and control littermates. It was shown that the potentiation of AMPAR-mediated EPSCs was significantly impaired in RNF220 depletion neurons (RNF220 KO, 239.69 ± 22.94% baseline; control, 442.02 ± 51.04% baseline; Fig. 3D). Together, all these data indicate that RNF220 regulates postsynaptic AMPAR expression to affect excitatory synaptic transmission and plasticity.

RNF220 directly ubiquitinates AMPARs to regulate excitatory synaptic activity

To test whether RNF220 regulates GluA1 and GluA2 receptor expression by modulating their polyubiquitination and then protein stability, we immunoprecipitated GluA1 or GluA2 from brain homogenates of *RNF220* cKO mice and control littermates, and checked their ubiquitination levels using a ubiquitin antibody. Both the endogenous GluA1 and GluA2 ubiquitination were markedly decreased in RNF220 cKO hippocampus (Fig. 4A) and cerebral cortex (fig. S4A), while their protein level input and immunoprecipitation were obviously increased.

These results lead us to speculate that AMPARs might be direct ubiquitination substrates of RNF220. To test this idea, we cotransfected Myc-RNF220 with hemagglutinin (HA)–GluA1, HA-GluA2, or HA-GluK2 into human embryonic kidney (HEK) 293 cells and first checked their interactions by coimmunoprecipitation assay. We found that RNF220 and GluA1 or GluA2 were coimmunoprecipitated when either RNF220 or GluA1/GluA2 was used as immunoprecipitation bait (Fig. 4, B and C). However, there was no detectable interaction between RNF220 and GluK2 (Fig. 4, B and C), a KAR subunit of glutamate receptor superfamilies and sharing similar topological architecture with AMPARs (*34*). As no commercial RNF220 antibody is available for in vivo immunoprecipitation analysis, we used an RNF220-BAP mouse model, in which RNF220 protein is fused with a biotin-accepting peptide (BAP), to examine the endogenous interactions between RNF220 and glutamate receptors in hippocampal (Fig. 4D) and cortical tissues (fig. S4B). When the BAP antibody was applied for immunoprecipitation, endogenous RNF220 was successfully immunoprecipitated from brain homogenates of RNF220-BAP mice but not control littermates. In addition, we found that only AMPAR subunits GluA1 and GluA2, but not NMDAR subunits GluN1, GluN2A, or GluN2B, were coimmunoprecipitated with RNF220 (Fig. 4D and fig. S4B) from tissue lysate of RNF220-BAP mice. These results suggest that RNF220 directly interacts with GluA1 and GluA2 receptors and regulates their protein stability.

To further test the idea that RNF220 directly ubiquitinates AMPARs, Myc-RNF220 was cotransfected with Flag-GluA1 or Flag-GluA2 into HEK293 cells. The polyubiquitination levels of both GluA1 (Fig. 4E) and GluA2 (Fig. 4F) were markedly increased by RNF220 co-overexpression (OE). Moreover, this kind of modification was dependent on its E3 ligase activity (Fig. 4, E and F), as RNF220-regulated ubiquitination of GluA1 or GluA2 was fully

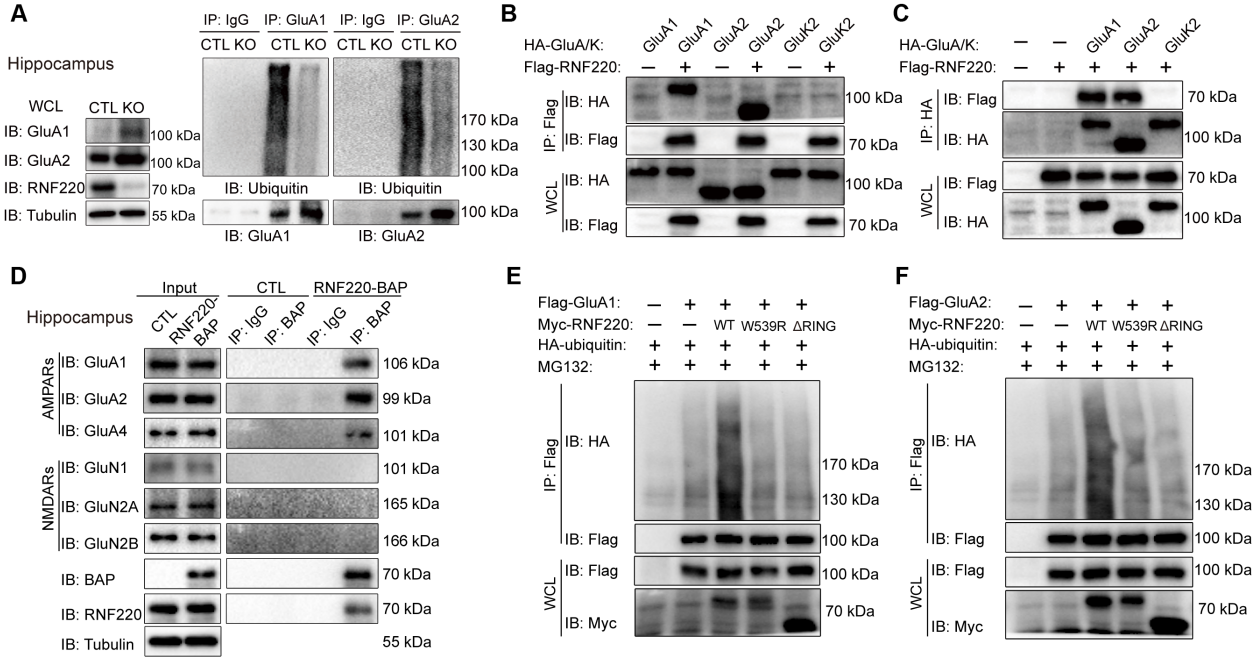

Fig. 4. RNF220 directly ubiquitinates AMPARs to regulate the receptor protein stability. (**A**) Polyubiquitination analyses of endogenous GluA1 and GluA2 protein in hippocampus of *Emx1-Cre;RNF220*$^{fl/fl}$ mice and littermate controls. (**B** and **C**) Coimmunoprecipitation analyses of Flag-tagged RNF220 or HA-tagged glutamate receptor interaction HEK293 cells with transfection as indicated. The whole-cell lysates (WCLs) were immunoprecipitated by Flag or HA antibody, and the WCLs and immunoprecipitations (IPs) were immunoblotted by the indicated antibodies. (**D**) Coimmunoprecipitation analyses of the interaction between RNF220 and glutamate receptors from RNF220-BAP and littermate mice hippocampus, and the input and IP samples were immunoblotted with the indicated antibodies. (**E** and **F**) Polyubiquitination analyses of GluA1 and GluA2 by coexpressed RNF220 or E3 ligase-dead mutants in HEK293 cells.

impaired when cotransfecting the ligase activity–diminished mutant (W539R; fig. S5, A and B). The above results indicate that AMPARs are direct ubiquitination substrates for RNF220.

To examine whether RNF220 regulates AMPAR-mediated excitatory synaptic transmission through such ubiquitination-dependent manner, wild-type RNF220 or the above ligase-dead mutants were individually overexpressed in CA1 neurons from rat hippocampal slice cultures by biolistic transfection (Fig. 5A). We found that AMPAR EPSCs were significantly decreased (RNF220 OE, 59.41 ± 11.29% WT; Fig. 5B), while the paired-pulse ratio did not change (control, 1.80 ± 0.16; RNF220 KO, 1.82 ± 0.17; Fig. 5C). However, the RNF220-mediated repression of synaptic activity was lost, while its E3 ligase activity was diminished [RNF220(W539R) OE, 95.39 ± 11.15% WT; RNF220(ΔRING) OE, 98.68 ± 18.77% WT; Fig. 5, D and E]. Moreover, different from RNF220 depletion (Fig. 3B), the two ligase-dead mutants failed to enhance AMPAR-mediated EPSCs, although they maintained the binding affinity with GluA1 and GluA2 subunits (fig. S4, C and D), suggesting that these two mutants might not have any dominant negative effect against endogenous RNF220 for the regulation of AMPAR expression. Unexpectedly, when RNF220 was depleted or overexpressed, we found that NMDAR-mediated EPSCs were modestly but significantly increased or decreased (fig. S3, A to D), respectively. Because our biochemical results indicated that there was no significant change of NMDAR subunit protein levels when RNF220 was lost (Fig. 2A and fig. S2A) and that, in slice cultures, the number of dendritic spines on CA1 pyramidal neurons was not changed significantly while depleting or overexpressing RNF220 (fig. S3, E and F), we presume that there might be other unknown targets for RNF220 that are involved in NMDAR synaptic regulation. Furthermore, the lack of direct interaction between RNF220 and NMDAR subunits further supports that the observed change of NMDAR EPSCs (fig. S3, A to D) is not attributed to direct modulation of the protein stability of NMDAR subunits by RNF220. Together, these results indicate that RNF220 is an E3 ubiquitin ligase for AMPARs to control protein stability and regulate excitatory synaptic transmission.

RNF220 regulation of synaptic activity involves ubiquitination of both GluA1 and GluA2 receptors

It is known that most of the PTMs for AMPAR subunits occur at the intracellular C-terminal domains (*3*, *6*), and we found that C termini of AMPARs were required for RNF220-mediated polyubiquitination, as truncation of either the GluA1 or GluA2 C terminus strongly diminished the enhanced ubiquitination level by RNF220 (fig. S5, A and B). We noted that there are four lysine sites (K814, K820, K823, and K869) or six lysine sites (K816, K822, K825, K828, K848, and K864) in mouse GluA1 or GluA2 C terminus for potential ubiquitination (Fig. 6A). To find out the determinant ubiquitination sites, we mutated these lysines into arginines individually and then examined RNF220-regulated polyubiquitination of each mutant. We found that K823/K868 of GluA1 and K825/K848/K864 of GluA2 were involved in each subunit's polyubiquitination (fig. S5, C and D). Furthermore, when these lysine sites were simultaneously mutated into arginines, RNF220 failed to enhance the polyubiquitination levels of the resulting mutants, GluA1 (2KR) [relative levels: GluA1(WT), 4.41 ± 0.41; GluA1(2KR), 1.08 ± 0.04; Fig. 6B] and

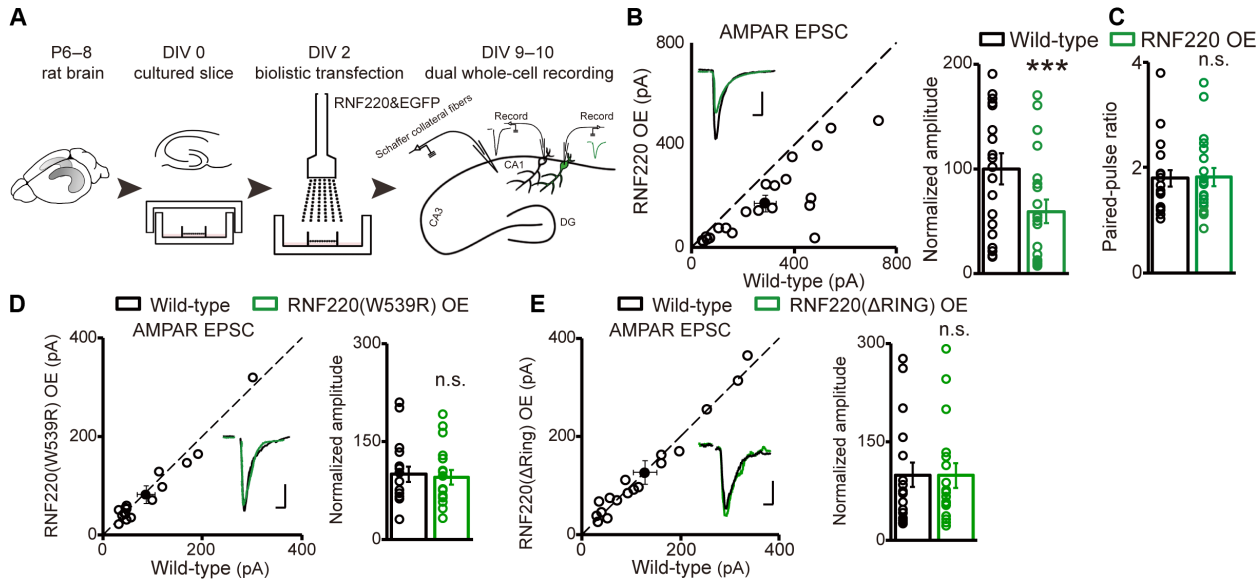

Fig. 5. The E3 ligase activity is essential for RNF220 regulating AMPAR-mediated synaptic transmission. (**A**) Schematic cartoon of the experimental workflows on rat hippocampal slices. (**B** to **E**) Regulation of AMPAR EPSCs by wild-type RNF220 [(B), $n = 21$], RNF220(W539R) [(D), $n = 17$], or RNF220(ΔRING) [(E), $n = 17$] overexpression in cultured hippocampal slices. Scatterplots show dual whole-cell eEPSCs, measured as in Fig. 3G, of a transfected CA1 pyramidal neuron (green trace) and a neighboring wild-type one (black trace). The scale bars for representative eEPSC traces are 150 pA/20 ms. Bar graphs (mean ± SEM) show normalized eEPSC amplitudes presented in scatterplots. Statistical analyses are compared to controls with two-tailed Wilcoxon signed-rank sum test. Paired-pulse ratios (mean ± SEM) of eEPSCs from wild-type ($n = 19$) and RNF220 OE ($n = 19$) neurons are shown in bar graphs overlaid with the actual data points (C), and statistical analyses are compared to controls with Mann-Whitney *U* test with Bonferroni correction. n.s., $P > 0.05$ and ***$P < 0.001$.

GluA2 (3KR) [relative levels: GluA2(WT), 4.72 ± 0.35; GluA2(3KR), 1.14 ± 0.01; Fig. 6C], suggesting that these lysines are direct ubiquitination sites.

Although both GluA1 and GluA2 can be ubiquitinated by RNF220 through direct protein interaction and this ubiquitination-dependent modification is involved in AMPAR-mediated synaptic transmission (Fig. 5), it is unclear whether RNF220 has any preference between these two subunits during synaptic regulation in hippocampal CA1 pyramidal neurons through such mechanism, as they are the two mostly expressed AMPAR subunits in such hippocampal cells (*35*). To address this question, RNF220 was cotransfected with wild-type GluA1 or GluA2, as well as GluA1 (2KR) or GluA2 (3KR) mutant, into hippocampal CA1 neurons. Because the eEPSCs would be rectified by GluA1 or GluA2(Q) homomeric receptors, if there is any such preference, the overexpressed AMPAR subunits and mutants would have different effects on the rectification index, which can be used as a measure of each receptor's synaptic trafficking ability. However, it was found that in the presence of RNF220, overexpression of either wild-type GluA1 or GluA2(Q) subunit did not rectify the AMPAR EPSCs, while the currents rectified to similar levels by GluA1 (2KR) [GluA1(WT) + RNF220, 103.02 ± 2.62% WT; GluA1(2KR) + RNF220, 65.56 ± 3.69% WT; Fig. 6D] and GluA2 (3KR) [GluA2(WT) + RNF220, 106.18 ± 2.62% WT; GluA2(3KR) + RNF220, 65.83 ± 2.31% WT; Fig. 6E]. These results suggest that RNF220 has no preference and degrades both wild-type GluA1 and GluA2 to the same extent.

RNF220-mediated ubiquitination is involved in AMPAR neuronal surface expression

To test whether the above ubiquitination-dependent regulatory mechanism is also involved in AMPAR surface expression, cellular surface levels of GluA1 and GluA2 subunits from *RNF220* cKO mice were examined through BS3 cross-linking–based immunoprecipitation analysis (*36*). We found that in the hippocampus (relative levels: GluA1, 3.03 ± 0.20; GluA2, 2.32 ± 0.32; Fig. 7A) and cerebral cortex (relative levels: GluA1, 2.61 ± 0.05; GluA2, 2.00 ± 0.22; Fig. 7B), surface expression levels of both GluA1 and GluA2 were increased. To further examine AMPAR surface expression, three guide RNAs (gRNAs) against rat *RNF220* were designed and their KO efficiencies (fig. S6, A and B) were tested by single-strand annealing (SSA) recombination-based luciferase assay (*37*). Moreover, reduction of endogenous RNF220 protein level by these gRNAs in B104 cells, a rat neuroma cell line, was confirmed through immunoblot assays (fig. S6, C and D). gRNA-1 was then transfected into rat primary cultured neurons, and surface expression of endogenous GluA1 receptors was examined by membrane-impermeable immunostaining. We found that the endogenous GluA1 levels on neuronal surface were increased after RNF220 depletion and then recovered by cotransfection of gRNA-resistant construct (EGFP, 100 ± 3.90; RNF220 gRNA, 133.98 ± 3.48; RNF220 gRNA+RNF220, 79.70 ± 3.36; Fig. 7C). In addition, overexpression of RNF220 suppressed GluA1 receptor level on neuronal surface, while its suppression ability was lost in the ubiquitination ligase-dead mutant, either RNF220(ΔRING) or RNF220(W539R) [relative levels: EGFP, 100 ± 7.11; RNF220, 65.80 ± 3.80; RNF220 (W539R), 80.08 ± 3.42; RNF220(ΔRING), 78.45 ± 3.42; Fig. 7D]. Because these two ligase-dead mutants failed to increase surface GluA1 levels as RNF220 KO, it further indicated that they might not have any dominant negative effect against endogenous RNF220. Together, these results indicate that the ubiquitination regulatory mechanism by RNF220 is also involved in neuronal surface expression of AMPARs.

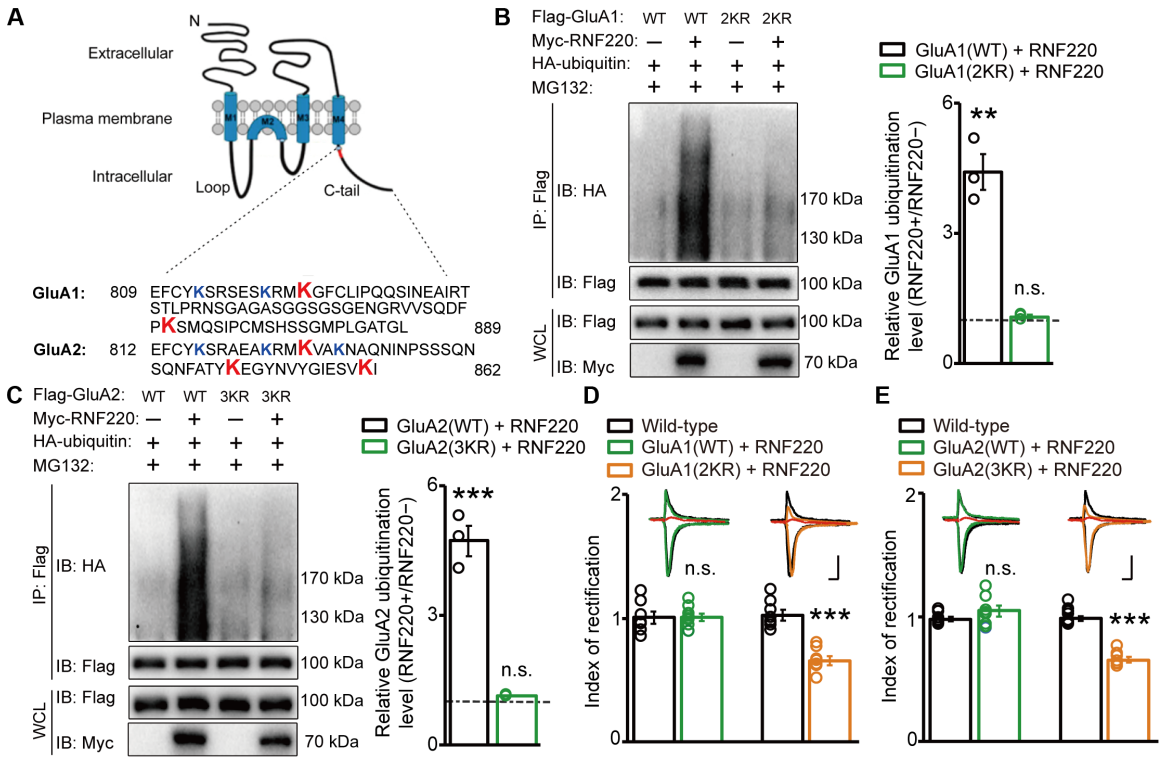

Fig. 6. RNF220 regulation of synaptic activity involves ubiquitination of both GluA1 and GluA2 receptors. (**A**) Schematic cartoon of AMPAR topological architecture and amino acid sequences of mouse GluA1 and GluA2 intracellular C termini. The lysine sites tested in polyubiquitination assays were highlighted with color, and the responsible ubiquitination lysine sites were highlighted in red. (**B** and **C**) Polyubiquitination analyses of exogenous GluA1(WT)/GluA1(2KR) mutant [(B), $n = 3$] and GluA2(WT)/GluA2(3KR) mutant [(C), $n = 3$] mediated by RNF220 in HEK293 cells with indicated transfection. Each input level of immunoprecipitated GluA1 or GluA2 was used for normalization of respective receptor's ubiquitination level. Bar graphs (mean ± SEM) show relative RNF220-regulated GluA1(WT), GluA1(2KR), GluA2(WT), and GluA2(3KR) ubiquitination levels normalized against each respective control without RNF220 transfection. Statistical analyses are compared to controls with unpaired *t* test. (**D** and **E**) Rectification analyses of AMPAR-mediated eEPSCs measured at −70, +40, and 0 mV sequentially. GluA1(WT) ($n = 8$), GluA1(2KR) ($n = 8$), GluA2(WT) ($n = 8$), or GluA2(3KR) ($n = 8$) was biolistically cotransfected with RNF220 into hippocampal CA1 pyramidal neurons, and wild-type neurons were used as controls. Representative traces are scaled and superimposed for comparison in the top panels. Scale bars, 100 pA/20 ms. Bar graphs (mean ± SEM) show rectification index of wild-type and indicated experimental neurons. Statistical analyses are compared to each wild-type controls with Mann-Whitney *U* test with Bonferroni correction. n.s., $P > 0.05$; ***$P < 0.001$; and **$P < 0.01$.

RNF220 forebrain KO mice show altered learning and memory behaviors

Our above results suggest that RNF220 is involved in the regulation of excitatory synaptic activity, and these findings lead us to investigate whether there is any behavioral dysfunction of the *RNF220* cKO mice. As forebrain is critical for processing information of high cognitive functions, we focused on the behaviors related to learning and memory. Morris water maze test was used to examine the spatial learning and memory ability. Unexpectedly, it was found that during the initial training period (day 1: control, 45.73 ± 3.78 s and RNF220 KO, 46.88 ± 1.94 s; day 2: control, 34.10 ± 6.90 s and RNF220 KO, 30.18 ± 4.99 s; day 3: control, 35.86 ± 3.31 s and RNF220, 28.59 ± 2.82 s; day 4: control, 28.34 ± 3.41 s and RNF220 KO, 25.31 ± 4.08 s; day 5: control, 29.5 ± 3.87 s and RNF220 KO, 20.92 ± 1.62 s; day 6: control, 27.18 ± 3.91 s and RNF220 KO, 16.71 ± 1.45 s; day 7: control, 19.16 ± 3.13 s and RNF220 KO, 17.57 ± 1.64 s; day 8: control, 16.89 ± 1.52 s and RNF220 KO, 14.63 ± 1.37 s; Fig. 8A), *RNF220* cKO mice took a lesser time to find the platform than did control mice on the fifth and sixth day, suggesting that the KO mice learn faster on these two days. However, there was no difference during the later training tests on the seventh and eighth day. Then, spatial memory was examined 1 day after the 8-day training, and it was shown that RNF220-deficient mice spent similar time in the target zone (control, 15.15 ± 1.95 s and RNF220 KO, 18.37 ± 1.70 s; Fig. 8B), suggesting normal spatial memory. In addition, there was no difference in the total swim distances (control, 1146 ± 58.70 cm and RNF220 KO, 1123 ± 33.16 cm; Fig. 8C) and swim speed (control, 19.78 ± 0.77 cm/s and RNF220 KO, 19.06 ± 0.56 cm/s; Fig. 8D) between the cKO and control mice. All these results indicate that lack of RNF220 affects mice spatial learning, but not memory.

We next examined contextual fear memory of *RNF220* cKO mice. During the fear conditioning, no difference was observed in the freezing time between control and KO mice (before shock: control, 2.50 ± 1.39% and RNF220 KO, 2.76 ± 0.95%; first: control, 15.11 ± 4.14% and RNF220 KO, 17.32 ± 4.28%; second: control, 38.54 ± 6.77% and RNF220 KO, 43.63 ± 5.46%; third: control, 67.54 ± 5.58% and RNF220 KO, 65.22 ± 4.84%; fourth: control, 81.30 ± 5.13% and RNF220 KO, 72.68 ± 6.10%; fifth: control, 87.05 ± 3.60% and RNF220 KO, 84.15 ± 3.18%; Fig. 8E). Compared to control littermates, freezing levels of forebrain *RNF220* cKO mice were reduced when tested 30 min after the conditioning (control, 62.55 ± 7.20% and RNF220 KO, 46.00 ± 4.23%; Fig. 8F), while both mouse lines

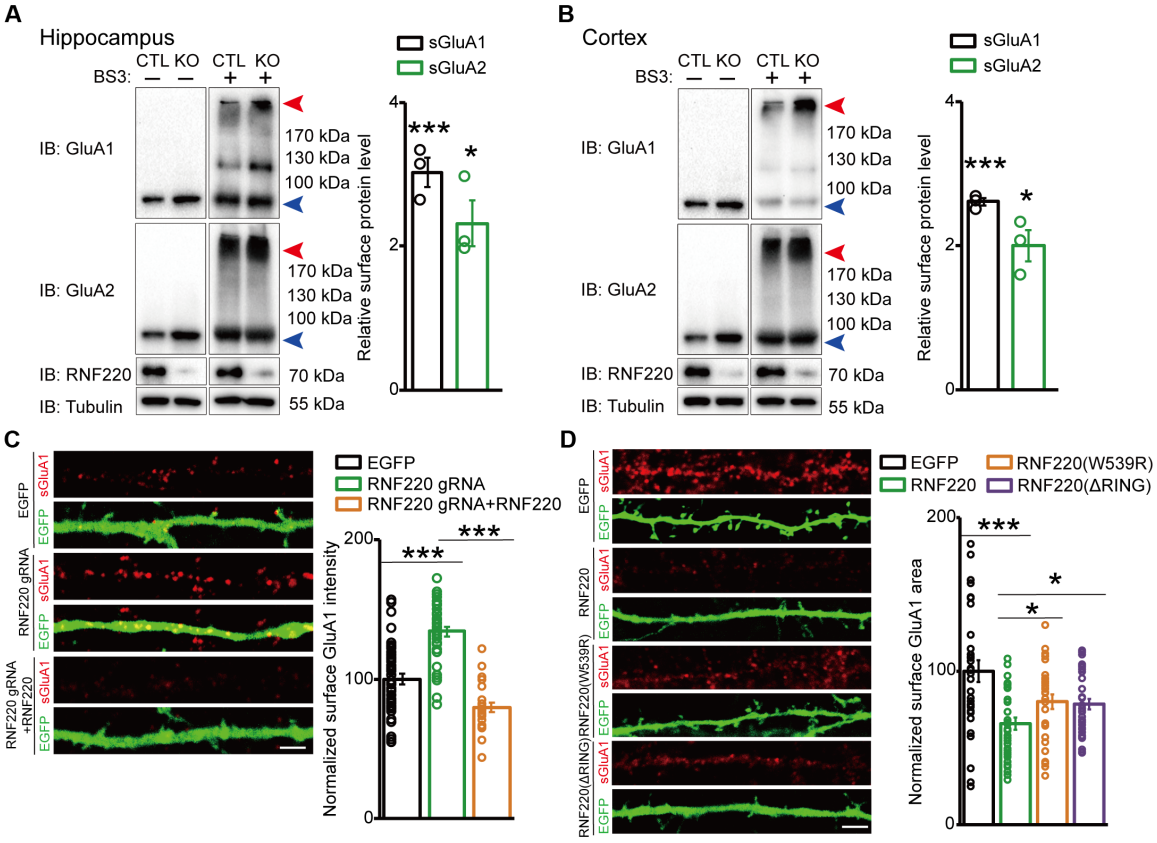

Fig. 7. RNF220-mediated ubiquitination is involved in AMPAR neuronal surface trafficking. (**A** and **B**) BS3 cross-linking assay of the surface expression of GluA1 and GluA2 from *Emx1-Cre;RNF220*$^{fl/fl}$ mice ($n = 3$) and littermate control ($n = 3$) hippocampal (A) and cortical (B) acute slices. The surface receptor levels (top band, red) are normalized against the cytoplasmic protein levels (bottom band, blue) as indicated. Bar graphs (mean ± SEM) show relative surface GluA1 and GluA2 (sGluA1 and sGluA2) protein levels normalized against each control with BS3 treatment. Statistical analyses are compared to controls with unpaired *t* test. (**C** and **D**) Impermeable immunofluorescence staining shows the cell surface GluA1 expression levels in primary cultured rat cortical neurons with indicated transfection. EGFP construct was coexpressed as marker for transfection. CRISPR-Cas9 was used for RNF220 KO, and gRNA-resistant RNF220 constructs were used for the rescue experiments. Bar graphs (mean ± SEM) show relative surface GluA1 intensity normalized against only EGFP transfection control [(C) EGFP, $n = 42$; RNF220 gRNA, $n = 39$; RNF220 gRNA + RNF220, $n = 26$; (D) EGFP, $n = 32$; RNF220, $n = 34$; RNF220(W539R), $n = 36$; RNF220(ΔRING), $n = 29$]. Statistical analyses are compared between indicated treatments with unpaired *t* test. Scale bars, 2.35 μm. ***$P < 0.001$ and *$P < 0.05$.

showed comparable freeze during the test on the first (control, 38.30 ± 4.61% and RNF220 KO, 36.47 ± 4.97%; Fig. 8G) or seventh (control, 26.40 ± 3.59% and RNF220 KO, 34.81 ± 4.12%; Fig. 8H) day after conditioning. These data suggest that the short-term fear memory of *RNF220* cKO mice is impaired, while the remote fear memory is intact. Furthermore, the novel object recognition test was used as another paradigm to examine the short-term memory in nonaversive condition. Consistently, while there was no significant difference of their exploring time (control, 37.66 ± 6.01 s and RNF220 KO, 32.00 ± 3.30 s; Fig. 8I), *RNF220* cKO mice showed less preference to novel object than control ones (control, 1.37 ± 0.21 and RNF220 KO, 0.25 ± 0.16; Fig. 8J).

In addition, we used the three-chamber social interaction test to examine social memory, which requires the ability of distinguishing familiar mice and stranger in a short interval. *RNF220* cKO mice showed a significant preference for the animated strangers over the inanimate balls to the same extent as the control littermates (Fig. 8K, preference: Control: Ball: 28.21 ± 2.59% and Str1: 71.79 ± 2.59%; RNF220 KO: Ball: 29.39 ± 2.88% and Str1: 70.61 ± 2.87%; Fig. 8L, social ratio: Control: 1.33 ± 0.05 and RNF220 KO: 1.24 ± 0.07). However, the cKO mice had a significant lower preference for the new strangers over the familiar strangers compared to the controls [preference: control, 23.99 ± 2.21% (Str1) and 76.01 ± 2.21% (Str2); RNF220 KO, 45.20 ± 2.95% (Str1) and 54.80 ± 2.95% (Str2); Fig. 8M; social ratio: control, 1.66 ± 0.04 and RNF220 KO, 0.24 ± 0.09; Fig. 8N], indicating a defect of the social memory. Together, all these results suggest that RNF220-deficient mice display altered behaviors of learning and memory.

Human pathogenic mutations impair RNF220 regulation of AMPARs

The patients harboring RNF220 substitutional mutations (R363Q and R365Q) exhibit symptoms of intellectual disability and seizures (*31*), which are related to malfunction of synaptic transmission. Therefore, we next investigated their effect on AMPAR ubiquitination and excitatory synaptic transmission. First, coimmunoprecipitation assay was used to test the interaction between the two RNF220 mutants and GluA1 [relative levels: RNF220(R363Q), 0.22 ± 0.05; RNF220(R365Q), 0.11 ± 0.02; Fig. 9A] or GluA2 (fig. S7A), and it was found that the binding affinity between RNF220 and

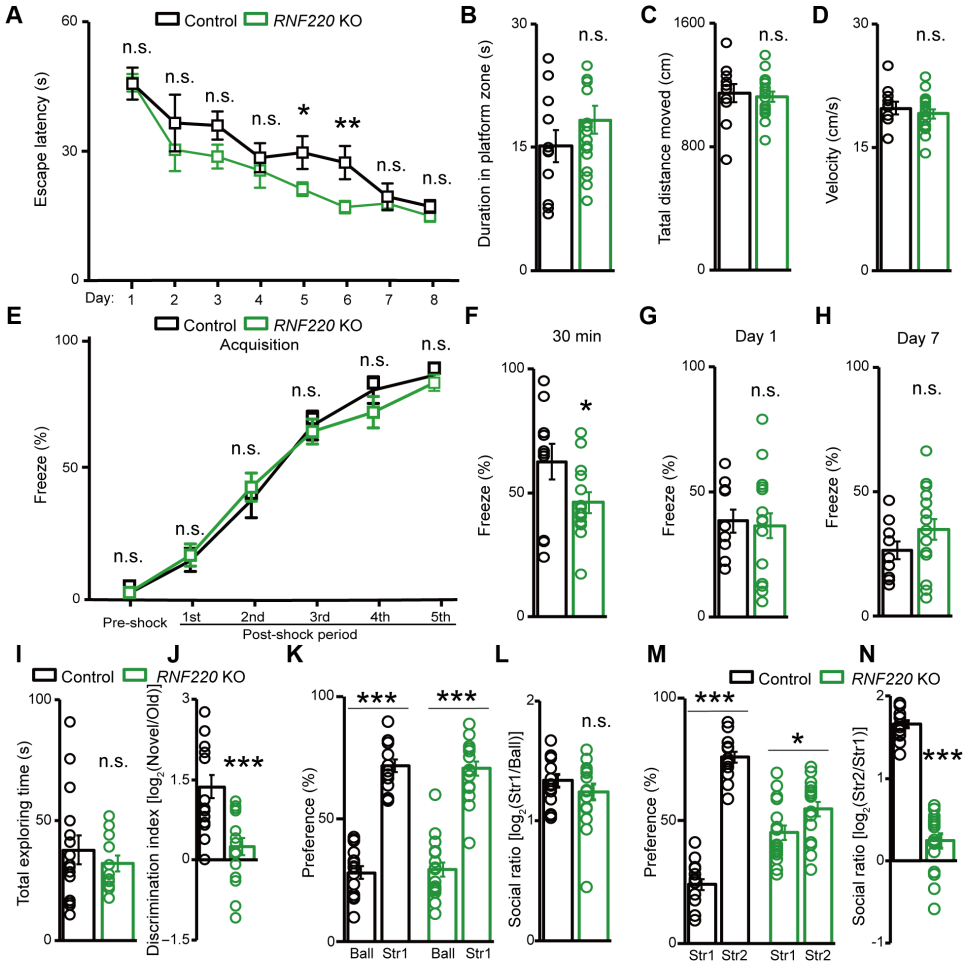

Fig. 8. *RNF220* forebrain KO mice show altered learning and memory behaviors. (**A** to **D**) Behavior analyses of Morris water maze test for *Emx1-Cre;RNF220*$^{fl/fl}$ mice ($n = 17$) and littermate controls ($n = 11$). (A) Escape latencies (mean ± SEM) to find the platform throughout the 8-day learning trials. (B to D) Spatial memory retrieval of these mice used in (A) was examined when the platform was removed. Bar graphs (mean ± SEM) show duration in platform zone (B), total traveled distances (C), and moving velocity (D). (**E** to **H**) Contextual fear conditioning analyses of *Emx1-Cre;RNF220*$^{fl/fl}$ mice ($n = 16$) and littermate controls ($n = 11$) by foot shock. (E) Percentage of freezing behavior (mean ± SEM) across fear conditioning sessions. (F to H) Fear memory of these mice used in (E) was tested by exposure to the environment only. Bar graphs (mean ± SEM) show percentage of freezing behavior 30 min (F), 1 day (G), and 7 days (H) after the contextual fear conditioning. (**I** and **J**) Novel object recognition test of *Emx1-Cre;RNF220*$^{fl/fl}$ mice ($n = 17$) and littermate controls ($n = 15$). Bar graphs (mean ± SEM) show total exploring time for new object (I) and logarithm of discrimination index (J). (**K** to **N**) Three-chamber sociability and social novelty test of *Emx1-Cre;RNF220*$^{fl/fl}$ mice ($n = 17$) and littermate controls ($n = 15$). Bar graphs (mean ± SEM) show normalized preference for inanimate ball and animated stranger (K), logarithm of sociability ratio (L), normalized preference for new and familiar animated stranger (M), and logarithm of sociability ratio (N). All statistical analyses are compared between indicated groups with unpaired *t* test. Str, stranger. n.s., $P > 0.05$; ***$P < 0.001$; and *$P < 0.05$.

AMPARs was strongly decreased by either R363Q or R365Q mutation. Consistently, these two missense variants showed markedly reduced ability to polyubiquitinate GluA1 [relative levels: RNF220(R363Q), 0.34 ± 0.05; RNF220(R365Q), 0.30 ± 0.02; Fig. 9B] and GluA2 receptors (fig. S7B). In addition, in primary cultured neurons, unlike wild-type RNF220, the enhanced surface expression of endogenous GluA1 receptors by CRISPR-mediated deletion of RNF220 could not be reversed by R363Q or R365Q RNF220 mutants [relative levels: EGFP, 100 ± 3.78; RNF220 KO, 142.37 ± 4.61; RNF220 KO + RNF220, 82.26 ± 3.39; RNF220 KO + RNF220(R363Q), 131.44 ± 4.21; RNF220 KO + RNF220(R365Q), 147.36 ± 3.42; Fig. 9C]. Last, in contrast to the wild-type RNF220 (Fig. 4G), the AMPAR-mediated EPSCs were not enhanced by overexpressing either mutant in CA1 neurons in slice cultures [RNF220(R363Q) OE, 97.15 ± 19.44% WT; RNF220(R365Q) OE, 103.08 ± 11.14% WT; Fig. 9, D and E]. Together, these results indicate that the two neuropathological mutations of RNF220 are involved in regulating ubiquitination of AMPARs and their expression on neuronal surface and synapse.

DISCUSSION

In this study, we find that RNF220 is an E3 ubiquitin ligase for AMPARs to repress their expression on neuronal surface and synapse. After RNF220 is depleted in forebrain neurons, the protein levels of GluA1 and GluA2 are increased and AMPAR-mediated synaptic activity is enhanced, while the cKO mice exhibit altered neural behaviors of learning and memory. Moreover, RNF220 with neuropathological-associated mutations loses its

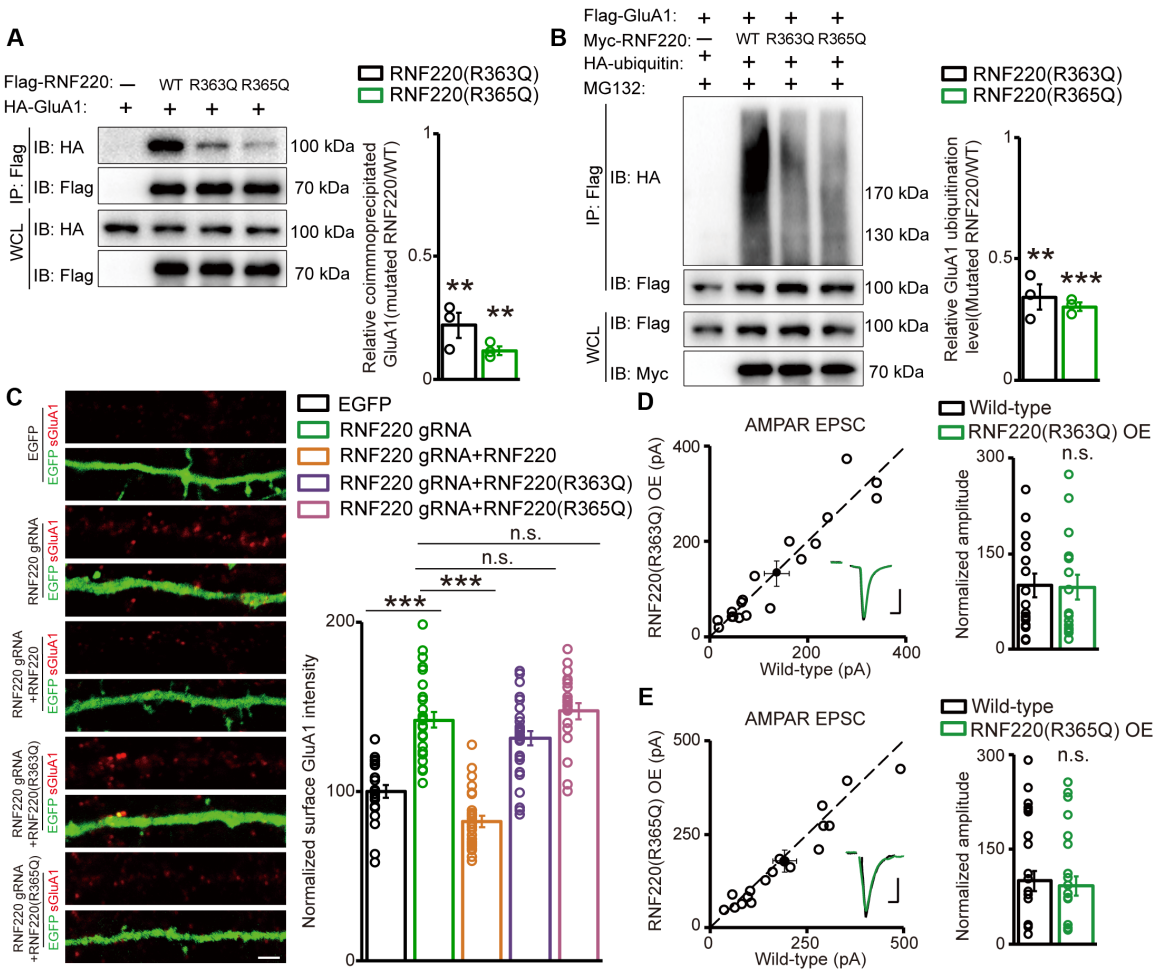

Fig. 9. Regulation of AMPARs by RNF220 is impaired by its human pathogenic mutations. (**A**) Coimmunoprecipitation analyses of GluA1 interaction with RNF220, RNF220(R363Q), or RNF220(R365Q). The WCLs were immunoprecipitated by Flag antibody, and the WCLs and IPs were immunoblotted by the indicated antibodies. Each input level of GluA1 in WCL was used for normalization of respective coimmunoprecipitated GluA1 level. The bar graph (mean ± SEM, $n = 3$) shows relative coimmunoprecipitated GluA1 levels normalized against the control levels in wild-type RNF220 immunoprecipitation. (**B**) Polyubiquitination analyses of GluA1 mediated by RNF220, RNF220(R363Q), or RNF220(R365Q). Each input level of immunoprecipitated GluA1 was used for normalization of respective GluA1 ubiquitination level. The bar graph (mean ± SEM, $n = 3$) shows relative GluA1 ubiquitination levels normalized against the control levels in wild-type RNF220 transfection. (**C**) Surface GluA1 trafficking regulated by RNF220 pathogenic mutants in primary cultured rat cortical neurons with indicated transfection. The bar graph (mean ± SEM) shows relative surface GluA1 intensity normalized against only EGFP transfection control [EGFP, $n = 22$; RNF220 gRNA, $n = 27$; RNF220 gRNA + RNF220, $n = 26$; RNF220 gRNA + RNF220(R363Q), $n = 30$; RNF220 gRNA + RNF220(R365Q), $n = 23$]. Scale bar, 2.35 μm. All these above statistical analyses are compared between indicated treatments with unpaired *t* test. (**D** and **E**) Regulation of AMPAR EPSCs by RNF220(R363Q) ($n = 18$) and RNF220(R365Q) ($n = 18$) overexpression in cultured hippocampal slices. The scale bars for representative eEPSC traces are 100 pA/20 ms. Bar graphs (mean ± SEM) show normalized eEPSC amplitudes presented in scatterplots. Statistical analyses are compared to respective controls with two-tailed Wilcoxon signed-rank sum test. n.s., $P > 0.05$; ***$P < 0.001$; and **$P < 0.01$.

ability to regulate AMPAR ubiquitination and the excitatory synaptic transmission.

The abundance of AMPARs at the synapse is crucial for synaptic efficiency and communication between neurons. AMPARs dynamically shuttle between the synapse and the extrasynaptic surface and cycle into and out of the neuronal plasma membrane (*1*–*3*). Numerous studies have revealed that PTMs on the intracellular C-tail domains of AMPAR subunits play crucial roles in these processes, and UPS-regulated AMPAR protein stability is involved in synaptic activity and plasticity (*3*, *6*, *7*). For AMPARs, four specific E3 ubiquitin ligases, named Nedd4, Nedd4L, APC^{Cdh1}, and RNF167, have been identified to regulate receptor surface and synaptic expression in primary cultured neurons (*13*, *19*–*22*). However, it is still unknown whether these ligases exert such regulation in the brain. Using a KO mice model, we have found that RNF220 is an E3 ubiquitin ligase for AMPARs and regulates endogenous AMPAR protein stability and synaptic expression in forebrain excitatory neurons. As AMPARs are widely expressed in the brain and the subunit composition of the tetrameric complex is different among different brain regions (*4*, *38*), it would be interesting to determine whether these ligases have any brain region specificity to regulate AMPAR ubiquitination and function. From the Allen Brain Atlas, it is shown that, in the adult mice, the genes of *Nedd4*, Fizzy-related protein 1 (FZR1; encoding APC^{Cdh1}), and *RNF220* are expressed broadly in the brain, while the expression levels of *Nedd4L* and *RNF167* are higher in the forebrain region (*30*). Here, we used

Emx1-Cre to specifically knock out RNF220 in the forebrain and found that RNF220 depletion leads to deregulated protein stability of AMPAR subunits GluA1 and GluA2 and caused alteration of learning and memory behaviors, suggesting that the loss of RNF220 in the forebrain neurons could not be compensated by the other E3 ligases. However, it is unknown whether the other E3 ligases have any redundancy or specificity for the regulation of AMPAR expression and related physiological functions when they are expressed in the same brain region. Further efforts are also needed to dissect their endogenous substrates of the AMPAR subunits in the brain and their involvement in neural behaviors.

The four GluA1-GluA4 subunits of AMPAR have diverse lengths and sequences of the C-terminal domains, and the corresponding PTMs are also quite different (*7*). Although it is reported that all the four subunits can be ubiquitinated at the C-terminal domains, only the specific E3 ubiquitin ligases for GluA1 and GluA2 have been identified (*18*). Nedd4, Nedd4L, and APC^{Cdh1} regulate GluA1 ubiquitination (*13*, *19*–*21*), while RNF167 regulates GluA2 ubiquitination (*22*). Moreover, it is still unknown whether these E3 ligases have any preference or specificity for these two subunits. For example, although RNF167 regulates surface expression of both GluA1 and GluA2 in neurons, only GluA2 ubiquitination has been examined (*22*). In this study, we have found that RNF220 interacts with both GluA1 and GluA2, and regulates both subunit ubiquitination and protein stability. Electrophysiological results showed that RNF220 modulates the synaptic expression of GluA1 and GluA2(Q) homomeric receptors to a similar extent. Therefore, we conclude that RNF220 is a specific E3 ubiquitin ligase for both GluA1 and GluA2 receptors and has no preference for the two subunits.

UPS-dependent protein stability regulation is an important way to remodel the postsynaptic components and is implicated in synaptic activity and plasticity. The proper control of postsynaptic protein quality is required for brain physiological procedures such as learning and memory, and dysfunction of the ubiquitination processes is known to be correlated with neuropsychiatric and neurodegenerative disorders (*9*, *10*, *39*). It has been estimated that 600 to 700 E3 ubiquitin ligase genes are present in the genome, and among them, 83 genes have been implicated in 70 different types of brain diseases (*40*). However, except for the extensively studied ones, such as PARKIN and UBE3A, the substrates of most of these E3 ubiquitin ligases, letting along the regulated biological processes, have remained elusive. Patients with the loss-of-function variants of the *FZR1* gene have developmental and epileptic encephalopathies associated with a spectrum of neonatal to childhood-onset seizure types, intellectual disability, developmental delay, and mild ataxia (*41*, *42*). However, the biological mechanisms underlying these symptoms and whether APC^{Cdh1}-mediated deregulation of AMPAR protein stability is involved in these pathological processes remain elusive. NEDD4L missense variants were identified in patients with periventricular nodular heterotopia, polymicrogyria, and developmental delay, and most have epilepsy (*43*–*47*). In addition, it has been revealed that the epilepsy-associated missense mutations impair Nedd4L-regulated GluA1 ubiquitination, thereby contributing to neuronal hyperactivity and seizures (*20*). RNF220 has been added to this list by a recent study showing that patients harboring two kinds of site mutation, R363Q and R365Q, exhibit several brain abnormalities, including leukodystrophy, ataxia, sensorineural deafness, corpus callosum agenesis, intellectual disability, and seizures (*31*). Note that these abnormalities are related to different brain regions and cell types, and RNF220 should regulate the respective biological processes through different ubiquitination targets and corresponding mechanisms. In this study, we have found that RNF220 in mice forebrain is required for the learning and memory performance, and AMPAR subunits GluA1 and GluA2 are direct ubiquitination substrates of RNF220. This UPS-dependent regulation is involved in the excitatory synaptic transmission and plasticity of hippocampal CA1 pyramidal neurons, and these disease mutations impair RNF220-regulated AMPAR ubiquitination and excitatory synaptic transmission. As malfunction of learning and memory is a major symptom and hippocampal functional connectivity is aberrant in intellectual disability individuals (*48*, *49*), the molecular mechanism that we revealed here might contribute to intellectual disability symptom of the above patients (*31*). However, more effort is required to dissect how the two mutations of RNF220 contribute to other symptoms of these patients. For example, white matter abnormality is another important clinical feature, and it would be interesting to study its function in oligodendrocyte cells or the molecular mechanism underlying its regulation of myelination.

MATERIALS AND METHODS

Ethics statement

All the protocols and procedures for the mice and rat studies were approved by the Animal Care and Use Committee of Kunming Institute of Zoology, Chinese Academy of Sciences (SMKX-20180523-129).

Animal procedures

All mice and rats were kept in individual ventilated cages in specific pathogen–free environment. All mice were maintained on a C57BL/6 background. Analysis was performed only after lines were crossed to C57BL/6 for at least three generations. *RNF220*$^{fl/fl}$ and *Emx1-Cre* mouse lines were described in our previous studies (*23*, *50*).

The stage of mouse or rat embryos was determined by taking the morning when the copulation plug was seen as embryonic day 0.5 (E0.5). All genotypes described were confirmed by PCR using genome DNAs prepared from tail tips as described previously (*23*, *50*). PCR-amplified DNA was analyzed on a 2% tris-borate EDTA agarose gel.

Plasmid construction

Flag- or Myc-tagged mouse wild-type or mutated RNF220 constructs were used as previously described (*24*). HA-tagged wild-type ubiquitin was a gift from C. Chen's laboratory of Kunming Institute of Zoology, China Academy of Sciences. pCAGGS-mRNF220-IRES-EGFP plasmids were used as previously described (*28*). HA-tagged mouse GluA1 and GluA2 mutants were subcloned into pCS2-N-HA vectors. Site mutation (lysine to arginine) of GluA1 and GluA2 mutants, gRNA-resistant RNF220 construct, and RNF220 mutations (R363Q and R365Q) were created through a site-directed mutation with PCR-driven overlap extension as previously described (*24*).

For RNF220 KO in primary cultured rat neurons, gRNAs against rat RNF220 were synthesized and cloned into pSpCas9(BB)-2A-GFP (PX458) vectors (Addgene, plasmid #48138). The three gRNA sequences used were as follows: gRNF220-1#, 5′-GCGAGTTGCAGGAACATATG-3′; gRNF220-2#, 5′-AGCGAGTTGCAGGAACATAT-3′; and gRNF220-3#, 5′-TCCCCGGCCAGGTAAGAAGA-3′.

Cell culture and transfection

Human HEK293 and rat neuroblastoma B104 cells were grown in Dulbecco's modified Eagle's medium (DMEM) supplemented with

10% fetal bovine serum, penicillin (100 U/ml), and streptomycin (100 mg/ml) and transfected by Lipofectamine 2000 (Invitrogen, catalog no. 11668019) according to the manufacturer's instructions.

Primary cultured cortical neurons were prepared from Sprague-Dawley rat embryos (E16.5 to E18.5). The heads of the embryos were immersed in ice-cold Hanks' buffered salt solution (HBSS; Gibco, catalog no. 14170112), and cortical tissue was isolated and digested with papain (1 mg/ml; Worthington, catalog no. LS003119) and deoxyribonuclease I (Sigma-Aldrich, catalog no. D4527) for 18 min at 37°C. Afterward, cortical tissues were homogenized and dissociated by trituration using a glass pipette and filter with 40-μm cell strainer. Neurons were plated in Neurobasal medium (Thermo Fisher Scientific, catalog no. 12348017) supplemented with 2% B27 (Thermo Fisher Scientific, catalog no. 12587010) and 1% GlutaMAX (Gibco, catalog no. 35050061) on 25-mm glass coverslips precoated with poly-D-lysine (Sigma-Aldrich, catalog no. P6407) and laminin (Sigma-Aldrich, catalog no. L2020). The cells were cultured in six-well plates, once every 4 days, and 700 μl of culture medium per well was replaced by 1000 μl of fresh medium. Neurons were transfected at DIV (days in vitro) 14 to DIV15 with Lipofectamine 3000 (Invitrogen, catalog no. L3000015) according to the manufacturer's instructions and fixed then stained 3 days after transfection.

The SSA recombination-based luciferase activity recovery assay was performed as previously described (*37*). Briefly, the luciferase SSA reporter, driven by the cytomegalovirus promoter, is composed of two truncated luciferase fragments, separated by recombination fragment with a homologous arm of 870 base pairs (bp) following a stop codon and a target exon around 500 bp, including the designed gRNA sequence in the middle. When double-strand break generated by Cas9/gRNA was repaired, the luciferase activity could be recovered (fig. S6A1). The cotransfection of plasmid expressing spCas9 and gRNA, SSA luciferase construct, and *Renilla* reporter into HEK293 cells was carried out in 24-well plates. Each experiment was repeated three times. Forty-eight hours after transfection, the cell lysate was obtained with luciferase cell lysis buffer and the relative luciferase activity was measured using a dual-luciferase assay system (Promega, catalog no. E1910) according to the manufacturer's instructions. The target sequence included the SSA luciferase reporter that was amplified by the following PCR primers using rat genome DNA as template: forward, 5′-GAATGTTTGTTGAATGACTGTAG-3′ and reverse, 5′-CAGACCCTGTACCTGCTTCTGTC-3′.

Hematoxylin and eosin staining, immunochemistry, and immunofluorescence assays

For hematoxylin and eosin staining assays, brains of *Emx1-Cre;RNF220$^{fl/fl}$* mice and littermate controls were carefully dissected and fixed in 4% paraformaldehyde (PFA) for at least 2 days. Cryostat sections were prepared as previously described (*23*). Fixed sections were used for hematoxylin and eosin staining by a kit from Solarbio (catalog no. G1120) according to the manufacturer's instructions.

For cell surface AMPAR staining, primary cultured cortical and hippocampal neurons were fixed in 4% PFA and blocked in 10% bovine serum albumin. Cells were then incubated with rabbit anti-GluA1 (Invitrogen, catalog no. 32-0300, 1:200) antibody at 4°C overnight and incubated with goat anti-mouse immunoglobulin G (IgG) Alexa Fluor 594 (1:400; Invitrogen, A11005) for 3 hours at room temperature. Immunoreactive signals were visualized, and images were obtained with a confocal microscope (FV1000, Olympus). To quantify positive immunostaining signals, traces were drawn using the Sholl analysis tool in ImageJ software. Then, immunoreactive signals ($n \geq 35$ for each group from three cultures) were counted and destined for statistical analysis.

Immunochemistry and immunofluorescence on brain sections were carried out as previously described (*23*). For immunostaining on tissue cryosections, transverse sections of 12 μm thickness were prepared. Sections were incubated with primary antibody at 4°C overnight, following the appropriate secondary antibody for 3 hours at room temperature. The sections were then processed using a VECTASTAIN Elite ABC kit (Vector Laboratories, catalog no. PK-6100) for 1 hour, and immunoreactivity was visualized by incubation with diaminobenzidine and H_2O_2. Sections were observed, and images were captured using an epifluorescence microscope (IX83, Olympus). The primary antibodies used in this study were anti- (1:200; Abcam, catalog no. ab18465), anti-Satb2 (1:200; Abcam, catalog no. ab69995), and anti-RNF220 (1:200; Sigma-Aldrich, catalog no. HPA027578).

Real-time PCR analysis

Cortex or hippocampus of *Emx1-Cre;RNF220$^{fl/fl}$* mice and littermate controls was homogenized, and total RNA was isolated using TRIzol reagent (TIANGEN, catalog no. DP424) according to the manufacturer's instructions. cDNA was synthesized using the First-Strand cDNA Synthesis Kit (Fermentas, catalog no. K1632) with random hexamers. Real-time reverse transcription PCR was performed using a Roche 480 Real-Time LightCycler system and LightCycler 480 SYBR Green I Master reagent (Roche, catalog no. 04707516001) with the following primers: mouse GluA1, 5′-AGGGATCGACATCCAGAGAG-3′ and 5′-TGCACATTTCCTGTCAAACC-3′; mouse GluA2, 5′-CAGTTTCGCAGTCACCAATG-3′ and 5′-ACCCAAAAATCGCATAGACG-3′; mouse GluN1, 5′-GGATACCAGATGTCCACCAGACTAAAG-3′ and 5′-AACGCAGAAGCCATAACAGCAC-3′; mouse GluN2A, 5′-CGGGTCTCATTTCAGTCTCTTACG-3′ and 5′-GGTTGTCATCTGGCTCACAGTCAG-3′; mouse GluN2B, 5′-GCGATTTGGTTACTCTGGGGTC-3′ and 5′-GTCTCTGGAACTTCTTGTCACTCAGG-3′; mouse β-actin, 5′-GCCAACCGTGAAAAGATGAC-3′ and 5′-GAGGCATACAGGGACAGCAC-3′; mouse PSD-95, 5′-CAAGGATGGCAGGTTGCAGATCGGA-3′ and 5′-TCCTCATGCATGACATCCTCTAG-3′; and mouse synaptophysin, 5′-GCAGCTACACCGGAGAGCTTCGGCT-3′ and 5′-GTACACTTGGTGCAGCCTGAATG-3′. β-Actin was used as the internal control.

Western blot and coimmunoprecipitation assays

Western blot and coimmunoprecipitation assays were carried out as previously described (*23*). The following primary antibodies were used: anti-Flag (1:5000; Sigma-Aldrich, catalog no. F7425), anti-Myc (1:5000; Proteintech, catalog no. 16286-1-AP), anti-HA (1:5000; Sigma-Aldrich, H3663), anti-RNF220 (1:1000; Sigma-Aldrich, catalog no. HPA027578), anti-GluA1 (1:1000; Cell Signaling Technology, catalog no. 13185S), anti-GluA2 (1:1000; Proteintech, catalog no. 11994-1-AP), anti-GluN1 (1:1000; Proteintech, catalog no. 27676-1-AP), anti-GluN2A (1:1000; Proteintech, catalog no. 19953-1-AP), anti-GluN2B (1:1000; Proteintech, catalog no. 21920-1-AP), anti-PSD-95 (1:1000; Proteintech, catalog no. 20665-1-AP), anti-synaptophysin (1:1000; Proteintech, catalog no. 17785-1-AP), anti-BAP (1:1000; Abcam, catalog no. AB97083), and anti–α-tubulin (1:5000; Proteintech, catalog no. 66031-1-lg). Horseradish peroxidase–coupled goat anti-mouse or rabbit antibodies were used as secondary antibody.

Total cell lysate and synaptosomal and PSD fractions were extracted from mouse cortex or hippocampus as described (*51*). Briefly, cortical or hippocampal tissues of *Emx1-Cre;RNF220*$^{fl/fl}$ mice and littermate controls were dissected and homogenized on ice in 10 volumes of cold sucrose buffer [0.32 M sucrose and 25 mM Hepes (pH 7.4)] with protease inhibitors. Homogenates were centrifuged at 710*g* for 10 min at 4°C to isolate supernatant from large debris and nuclei. The supernatant fraction was centrifuged at 10,000*g* for 15 min at 4°C; then, the supernatant containing light membrane and cytosolic fraction was discarded, and the pellets were washed twice with cold sucrose buffer and resuspended in cold Hepes-buffered saline (HBS) containing 25 mM Hepes and 150 mM NaCl (pH 7.4) to obtain synaptosome fractions. PSD-enriched fractions were prepared by solubilizing synaptosomes in 1% Triton X-100 (HBS) at 4°C for 30 min and, subsequently, centrifuging at 10,000*g* for 20 min. The pellet was resuspended in 3% SDS in HBS to yield PSD-enriched fractions.

Total protein concentration in brain homogenates or cell lysates was measured using a bicinchoninic acid assay (BCA) system (Thermo Fisher Scientific, catalog no. 23227). Protein lysates were boiled in SDS loading buffer, and equivalent protein quantities (30 to 100 μg) were resolved by SDS–polyacrylamide gel electrophoresis (SDS-PAGE) and Western blotting, whereby blots were probed with primary antibodies and immunoreactive bands were quantified using ImageJ software.

BS3 cross-linking assay

BS3 cross-linking assay was carried out as previously described (*36*). Mouse brain slices of 250 μm thickness from *Emx1-Cre;RNF220*$^{fl/fl}$ mice and littermate controls were prepared in ice-cold solution bubbled with 95% O_2/5% CO_2 consisting of the following: 2.5 mM KCl, 1.25 mM NaH_2PO_4, 10 mM $MgSO_4$, 0.5 mM $CaCl_2$, 26 mM $NaHCO_3$, 11 mM glucose, and 234 mM sucrose. Then, the cell membrane–impermeable BS3 cross-linker [Thermo Fisher Scientific, catalog no. 21580; 52 mM stock solution in 5 mM sodium citrate buffer (pH 5)] was added onto mouse brain slices at a final concentration of 2 mM and incubated for 30 min at 4°C with gentle agitation. Glycine (100 mM) was then added for 10 min at 4°C to quench the remaining unbound BS3. Cortex and hippocampus were isolated from those slices and then homogenized in lysis buffer [50 mM tris-HCl (pH 7.5), 150 mM NaCl, 1 mM EDTA, 1% SDS, and protease inhibitor cocktail] for 1 hour at room temperature. After sonication and centrifugation at 16,000*g* for 15 min, protein concentration was measured using the BCA protein assay. Proteins were resolved on 6% acrylamide SDS-PAGE gels and blotted for GluA1 and GluA2. Internal control α-tubulin was included for blotting to ensure that intracellular proteins were not BS3 cross-linked. Bands were quantified using ImageJ software. A surface/intracellular ratio was performed to analyze the levels of surface GluA1 and GluA2 expression.

Electrophysiological recording using acute and culture slices

Acute hippocampal slices were prepared from *Emx1-Cre;RNF220*$^{fl/fl}$ mice and littermate controls of P18 to P21 as previously described (*52*). Briefly, mice were anesthetized with isoflurane and 300-μm transverse hippocampal slices were cut using the Leica VT1200 Vibratome in chilled high-sucrose cutting solution consisting of the following: 2.5 mM KCl, 0.5 mM $CaCl_2$, 7 mM $MgCl_2$, 1.25 mM NaH_2PO_4, 25 mM $NaHCO_3$, 7 mM D-glucose, 210 mM sucrose, and 1.3 mM ascorbic acid. The slices were then incubated for 30 min at 34°C in artificial cerebrospinal fluid (ACSF) containing the following: 119 mM NaCl, 2.5 mM KCl, 26.2 mM $NaHCO_3$, 1 mM NaH_2PO_4, and 11 mM D-glucose. For acute slices, 2.5 mM $CaCl_2$ and 1.3 mM $MgSO_4$ were added into the ACSF, which was bubbled with 95% O_2/5% CO_2 to maintain pH, and the slices were allowed to recover at room temperature for 30 min to 1 hour before recording at room temperature. Organotypic hippocampal culture slices were obtained from P6 to P8 rats as previously described (*52*). Biolistic transfections were accomplished on DIV2 by Helios Gene Gun (Bio-Rad) with 1-μm DNA-coated gold particles. Slices were cultured at 34°C with medium, including 49% MEM (Gibco, catalog no. 12360-038), 25% HBSS (Gibco, catalog no. 14170-112), 25% donor equine serum (HyClone, catalog no. SH30074), 1% penicillin-streptomycin (Gibco, catalog no. 15140122), and 200 mM L-glutamine (Gibco, catalog no. 25030-149). On DIV8 before recording, organotypic hippocampal culture slices were transferred to ACSF supplemented with 4 mM $CaCl_2$ and 4 mM $MgSO_4$ and bubbled with 95% CO_2/5% O_2.

For recording, individual slices were transferred to a chamber mounted in an Olympus BX51WI upright microscope and perfused with ACSF (2.5 ml/min) supplemented with 100 μM picrotoxin and 4 μM 2-chloroadenosine. Simultaneous dual whole-cell recordings were made between EGFP-positive experimental cells as identified by epifluorescence and neighboring nontransfected control cells. Pyramidal neurons were identified by morphology and location. The internal recording solution contained the following:135 mM $CsMeSO_4$, 8 mM NaCl, 10 mM Hepes, 0.3 mM EGTA, 5 mM QX314-Cl, 4 mM Mg–adenosine triphosphate, 0.3 Na–guanosine triphosphate, and 0.1 spermine. Osmolarity was adjusted to 290 to 295 mOsm, and pH was buffered at 7.3 to 7.4. AMPAR-mediated responses were isolated by voltage-clamping the cell at −70 mV, whereas NMDAR-mediated responses were recorded at +40 mV, with amplitudes measured 100 ms after stimulation to avoid contamination by AMPAR current. A bipolar stimulation electrode was placed in stratum radiatum, and responses were evoked at 0.2 Hz. mEPSCs were recorded at −70 mV with 100 μM picrotoxin and 0.5 μM tetrodotoxin in the ACSF. LTP was induced by stimulating at 2 Hz for 90 s while clamping the cell at 0 mV, after recording a stable 3- to 5-min baseline, but not more than 6 min after breaking into the cell. To minimize run-up of baseline responses during LTP, slices were stimulated for ~10 min before breaking in, and both cells were held as cell-attached for 2 to 5 min before breaking into the whole-cell mode. Before breaking in, stimulation intensity was calibrated just below the threshold required to elicit an action potential from the recorded neurons. To ensure stable recording, membrane holding current, pipette series resistance, and input resistance were monitored throughout the recording. Whole-cell electrophysiological signals were collected with a MultiClamp 700B amplifier (Axon Instruments), filtered at 2 kHz, and digitized at 10 kHz. Data were analyzed offline with custom software (Igor Pro).

AAV injection

Newborn mouse pups (P0) were anesthetized on ice for 5 min and then mounted in a custom ceramic mold to make the head level in the *x* and *y* axes. Lambda was set as (*x*, *y*) = (0, 0). Zero point of *z* axis was the position that the injecting needle penetrated the skin. About 30 nl of viral solution was injected at each of the seven sites, (*x*, *y*, *z*) = (1.2, 1.2, 1.4/1.0/0.6) and (1.5, 1.0, 1.7/1.3/0.9/0.5), where the hippocampus was targeted at each cerebral hemisphere with microsyringe (Sutter Instrument) and a beveled glass injection pipette.

Injected pups were returned to home cage and used for acute slice preparation and electrophysiological recording 18 to 21 days afterward.

Mouse behavioral analyses

All the neural behavioral experiments were approved by the Animal Care and Use Committee of Kunming Institute of Zoology, Chinese Academy of Sciences. All behavioral experiments were performed in the light phase (9:00 a.m. to 6:00 p.m.) in a soundproof room with a neutral environment, and individual tests were performed in relatively fixed time. Male mice from seven litters were used for behavior analyses over the age of 2 months, and there were 2 or 3 days for resting between different tests. All mice were given a 60-min habituation after transferring to the behavioral test room. The experimenter was blind to the group identity of the tested mice, and the inner surfaces of instruments were cleaned with 75% alcohol after each test. Mice with different genotypes were conducted in random order. For all animals, each behavior was tested in the following order with a 7-day break in between: new object recognition, three-chamber social interaction, Morris water maze, and contextual fear conditioning.

Novel object recognition

The novel object recognition test was performed at P40 to P45. The test consisted of three phases: habituation, training, and test. In the habituation phase, the animals were allowed to explore an empty arena (a Plexiglas arena measuring 40 cm × 40 cm × 40 cm) for 5 min. Then, 24 hours later, on the training trial, each mouse was individually placed into the arena containing two identical objects (A1 and A2), equidistant from each other, and allowed to explore the objects for 10 min. After 1 hour, during the test phase, one copy of the familiar object (A3) and a novel object (B) was placed in the same location as during the training trial. The exploring time was recorded when the mouse touched the object with the tip of its nose or the front paws in a total time of 5 min. The discrimination index was calculated as the difference in time exploring the novel and the familiar objects, expressed as the percentage ratio of the total time spent exploring both objects.

Three-chamber social interaction

Sociability and social novelty tests were performed on mice as previously described with minor modifications (*53*). Both strangers used were wild-type C57BL/6 mice with matched age, body weight, and sex to the mice being tested. The social test apparatus was made of a clear glass box (90 cm × 50 cm × 30 cm, $L \times W \times H$) with three equally divided chambers (30 cm × 50 cm × 30 cm each). The chambers were interconnected with 5 cm × 5 cm openings, which could be opened or closed manually. The inverted cylindrical wire cups, which contain the stranger mouse or an object (ping-pong ball), were 10 cm in height and contained a 10-cm floor with the metal bars spaced 0.8 cm apart. The day before the test, each of the stranger mice was habituated inside the inverted wire cups, and each of the test mice was habituated to the apparatus with two empty wire cups inside the box for 15 min. On the test day, during the habituation phase, an empty wire cup was placed into the left and right chamber, and the tested mouse was placed into the center chamber and allowed to explore for 10 min, with all doors open between chambers. During the sociability test phase, an unfamiliar mouse (S1) was placed inside the inverted wire cup in one of the side chambers, an object (O) was placed inside the inverted wire cup on another side chamber, and the test mouse was introduced to the center chamber with the doors to both side chambers closed. A weighted water bottle was placed on each top of the inverted wire cup to prevent the mice from escaping. Note that an identical water bottle was also placed on the wire cup containing the object. Then, the doors between chambers were lifted simultaneously, and the test mouse was allowed to explore all three chambers for 10 min. During the social novelty test phase, the test mouse was placed in the central chamber with all doors closed between chambers. After a novel mouse (S2) was introduced in the inverted wired cup, replacing the object (O) in one of the side chambers, the doors between chambers were lifted simultaneously, and the test mouse was allowed to explore all three chambers for an additional 10 min. Time spent in close proximity to the empty cup (E1 and E2) or the stranger mice (S1 and S2) or object (O) was analyzed.

Morris water maze

To assess spatial learning and memory, the Morris water maze test was performed as described previously (*54*). Briefly, the blue circular pool was 120 cm in diameter and was divided into four equal quadrants with two hypothetical crossed lines. The hidden circular platform located in the middle of the target quadrant was 10 cm in diameter and submerged 1 cm below the water surface. During the training period, mice were trained to find the hidden platform over eight consecutive days with four trials everyday using a semirandom set of start locations, with the restriction that one trial each day was from each of the four different starting positions. If a mouse failed to find the platform within 60 s, it was picked up and placed on the platform for 20 s. On the ninth day, 24 hours after the last training session, the platform was removed, and 60 s was given to each mouse to search for the platform in the pool, with the starting location opposite to the previous position. The movement of the mice was monitored using Noldus software (EthoVision XT 8.0, Noldus Technology). Escape latency to find the platform, total distance moved, average velocity, total distance to platform, and duration in platform zone were automatically analyzed by the software.

Contextual fear conditioning

The contextual fear conditioning test was conducted as previously described with minor modifications (*54*). Mice were placed in a box and received five foot shocks (1.2 mA, 2 s) with 2-min intershock intervals by FreezeFrame (Coulbourn Instruments). Freezing behavior was measured by the amount of time mice exhibited freezing behavior during each intershock interval. Then, mice were placed back in the box (fear context) 30 min, 1 day, and 7 days after fear conditioning, and their contextual freezing behavior was measured for 11 min without any foot shocks applied.

Statistical analysis

For biochemical analysis, all experiments were repeated at least three times and differences between two treatments were assessed by unpaired *t* test. Significance of the difference between dual whole cell–recorded EPSCs from the experimental and control cells was determined using two-tailed Wilcoxon signed-rank sum test. For the experiments involving unpaired data, including the mEPSC parameters, paired-pulse ratios, and spine density, Mann-Whitney *U* test with Bonferroni correction for multiple comparisons was used. For animal neural behaviors, differences between experimental and control mice were assessed by unpaired *t* test. Data analysis was carried out in Igor Pro (WaveMetrics), Excel (Microsoft), and GraphPad Prism (GraphPad Software). Unless otherwise specified, there is no sample or data point excluded or omitted for the analysis reported in this study.

SUPPLEMENTARY MATERIALS

Supplementary material for this article is available at https://science.org/doi/10.1126/sciadv.abq4736

View/request a protocol for this paper from *Bio-protocol*.

REFERENCES AND NOTES

1. R. L. Huganir, R. A. Nicoll, AMPARs and synaptic plasticity: The last 25 years. *Neuron* **80**, 704–717 (2013).
2. R. A. Nicoll, A brief history of long-term potentiation. *Neuron* **93**, 281–290 (2017).
3. G. H. Diering, R. L. Huganir, The AMPA receptor code of synaptic plasticity. *Neuron* **100**, 314–329 (2018).
4. J. M. Henley, K. A. Wilkinson, Synaptic AMPA receptor composition in development, plasticity and disease. *Nat. Rev. Neurosci.* **17**, 337–350 (2016).
5. H. Zhang, C. R. Bramham, Bidirectional dysregulation of AMPA receptor-mediated synaptic transmission and plasticity in brain disorders. *Front. Synaptic. Neurosci.* **12**, 26 (2020).
6. W. Lu, K. W. Roche, Posttranslational regulation of AMPA receptor trafficking and function. *Curr. Opin. Neurobiol.* **22**, 470–479 (2012).
7. M. P. Lussier, A. Sanz-Clemente, K. W. Roche, Dynamic regulation of N-methyl-d-aspartate (NMDA) and α-amino-3-hydroxy-5-methyl-4-isoxazolepropionic acid (AMPA) receptors by posttranslational modifications. *J. Biol. Chem.* **290**, 28596–28603 (2015).
8. M. D. Ehlers, Activity level controls postsynaptic composition and signaling via the ubiquitin-proteasome system. *Nat. Neurosci.* **6**, 231–242 (2003).
9. J. H. Schwartz, Ubiquitination, protein turnover, and long-term synaptic plasticity. *Sci. STKE* **2003**, pe26 (2003).
10. A. M. Mabb, M. D. Ehlers, Ubiquitination in postsynaptic function and plasticity. *Annu. Rev. Cell Dev. Biol.* **26**, 179–210 (2010).
11. J. Widagdo, S. Guntupalli, S. E. Jang, V. Anggono, Regulation of AMPA receptor trafficking by protein ubiquitination. *Front. Mol. Neurosci.* **10**, 347 (2017).
12. N. Zheng, N. Shabek, Ubiquitin ligases: Structure, function, and regulation. *Annu. Rev. Biochem.* **86**, 129–157 (2017).
13. L. A. Schwarz, B. J. Hall, G. N. Patrick, Activity-dependent ubiquitination of GluA1 mediates a distinct AMPA receptor endocytosis and sorting pathway. *J. Neurosci.* **30**, 16718–16729 (2010).
14. M. P. Lussier, Y. Nasu-Nishimura, K. W. Roche, Activity-dependent ubiquitination of the AMPA receptor subunit GluA2. *J. Neurosci.* **31**, 3077–3081 (2011).
15. C. H. Na, D. R. Jones, Y. Yang, X. Wang, Y. Xu, J. Peng, Synaptic protein ubiquitination in rat brain revealed by antibody-based ubiquitome analysis. *J. Proteome Res.* **11**, 4722–4732 (2012).
16. S. A. Wagner, P. Beli, B. T. Weinert, C. Scholz, C. D. Kelstrup, C. Young, M. L. Nielsen, J. V. Olsen, C. Brakebusch, C. Choudhary, Proteomic analyses reveal divergent ubiquitylation site patterns in murine tissues. *Mol. Cell. Proteomics* **11**, 1578–1585 (2012).
17. J. Widagdo, Y. J. Chai, M. C. Ridder, Y. Q. Chau, R. C. Johnson, P. Sah, R. L. Huganir, V. Anggono, Activity-dependent ubiquitination of GluA1 and GluA2 regulates AMPA receptor intracellular sorting and degradation. *Cell Rep.* **10**, 783–795 (2015).
18. M. S. Goo, S. L. Scudder, G. N. Patrick, Ubiquitin-dependent trafficking and turnover of ionotropic glutamate receptors. *Front. Mol. Neurosci.* **8**, 60 (2015).
19. A. Lin, Q. Hou, L. Jarzylo, S. Amato, J. Gilbert, F. Shang, H. Y. Man, Nedd4-mediated AMPA receptor ubiquitination regulates receptor turnover and trafficking. *J. Neurochem.* **119**, 27–39 (2011).
20. J. Zhu, K. Y. Lee, K. A. Jewett, H. Y. Man, H. J. Chung, N. P. Tsai, Epilepsy-associated gene Nedd4-2 mediates neuronal activity and seizure susceptibility through AMPA receptors. *PLOS Genet.* **13**, e1006634 (2017).
21. A. K. Fu, K. W. Hung, W. Y. Fu, C. Shen, Y. Chen, J. Xia, K. O. Lai, N. Y. Ip, APC(Cdh1) mediates EphA4-dependent downregulation of AMPA receptors in homeostatic plasticity. *Nat. Neurosci.* **14**, 181–189 (2011).
22. M. P. Lussier, B. E. Herring, Y. Nasu-Nishimura, A. Neutzner, M. Karbowski, R. J. Youle, R. A. Nicoll, K. W. Roche, Ubiquitin ligase RNF167 regulates AMPA receptor-mediated synaptic transmission. *Proc. Natl. Acad. Sci. U.S.A.* **109**, 19426–19431 (2012).
23. P. Ma, N. N. Song, Y. Li, Q. Zhang, L. Zhang, Q. Kong, L. Ma, X. Yang, B. Ren, C. Li, X. Zhao, Y. Xu, X. Gao, Y. Q. Ding, B. Mao, Fine-tuning of Shh/Gli signaling gradient by non-proteolytic ubiquitination during neural patterning. *Cell Rep.* **28**, 541–553.e4 (2019).
24. P. Ma, X. Yang, Q. Kong, C. Li, S. Yang, Y. Li, B. Mao, The ubiquitin ligase RNF220 enhances canonical Wnt signaling through USP7-mediated deubiquitination of β-Catenin. *Mol. Cell. Biol.* **34**, 4355–4366 (2014).
25. J. Kim, T. I. Choi, S. Park, M. H. Kim, C. H. Kim, S. Lee, Rnf220 cooperates with Zc4h2 to specify spinal progenitor domains. *Development* **145**, dev165340 (2018).
26. P. Ma, T. An, L. Zhu, L. Zhang, H. Wang, B. Ren, B. Sun, X. Zhou, Y. Li, B. Mao, RNF220 is required for cerebellum development and regulates medulloblastoma progression through epigenetic modulation of Shh signaling. *Development* **147**, dev188078 (2020).
27. P. Ma, N. N. Song, X. Cheng, L. Zhu, Q. Zhang, L. L. Zhang, X. Yang, H. Wang, Q. Kong, D. Shi, Y. Q. Ding, B. Mao, ZC4H2 stabilizes RNF220 to pattern ventral spinal cord through modulating Shh/Gli signaling. *J. Mol. Cell Biol.* **12**, 337–344 (2020).
28. N. N. Song, P. Ma, Q. Zhang, L. Zhang, H. Wang, L. Zhu, C. H. He, B. Mao, Y. Q. Ding, Rnf220/Zc4h2-mediated monoubiquitylation of Phox2 is required for noradrenergic neuron development. *Development* **147**, dev185199 (2020).
29. P. Ma, Y. Li, H. Wang, B. Mao, Haploinsufficiency of the TDP43 ubiquitin E3 ligase RNF220 leads to ALS-like motor neuron defects in the mouse. *J. Mol. Cell Biol.* **13**, 374–382 (2021).
30. E. S. Lein, M. J. Hawrylycz, N. Ao, M. Ayres, A. Bensinger, A. Bernard, A. F. Boe, M. S. Boguski, K. S. Brockway, E. J. Byrnes, L. Chen, L. Chen, T. M. Chen, M. C. Chin, J. Chong, B. E. Crook, A. Czaplinska, C. N. Dang, S. Datta, N. R. Dee, A. L. Desaki, T. Desta, E. Diep, T. A. Dolbeare, M. J. Donelan, H. W. Dong, J. G. Dougherty, B. J. Duncan, A. J. Ebbert, G. Eichele, L. K. Estin, C. Faber, B. A. Facer, R. Fields, S. R. Fischer, T. P. Fliss, C. Frensley, S. N. Gates, K. J. Glattfelder, K. R. Halverson, M. R. Hart, J. G. Hohmann, M. P. Howell, D. P. Jeung, R. A. Johnson, P. T. Karr, R. Kawal, J. M. Kidney, R. H. Knapik, C. L. Kuan, J. H. Lake, A. R. Laramee, K. D. Larsen, C. Lau, T. A. Lemon, A. J. Liang, Y. Liu, L. T. Luong, J. Michaels, J. J. Morgan, R. J. Morgan, M. T. Mortrud, N. F. Mosqueda, L. L. Ng, R. Ng, G. J. Orta, C. C. Overly, T. H. Pak, S. E. Parry, S. D. Pathak, O. C. Pearson, R. B. Puchalski, Z. L. Riley, H. R. Rockett, S. A. Rowland, J. J. Royall, M. J. Ruiz, N. R. Sarno, K. Schaffnit, N. V. Shapovalova, T. Sivisay, C. R. Slaughterbeck, S. C. Smith, K. A. Smith, B. I. Smith, A. J. Sodt, N. N. Stewart, K. R. Stumpf, S. M. Sunkin, M. Sutram, A. Tam, C. D. Teemer, C. Thaller, C. L. Thompson, L. R. Varnam, A. Visel, R. M. Whitlock, P. E. Wohnoutka, C. K. Wolkey, V. Y. Wong, M. Wood, M. B. Yaylaoglu, R. C. Young, B. L. Youngstrom, X. F. Yuan, B. Zhang, T. A. Zwingman, A. R. Jones, Genome-wide atlas of gene expression in the adult mouse brain. *Nature* **445**, 168–176 (2007).
31. A. Sferra, P. Fortugno, M. Motta, C. Aiello, S. Petrini, A. Ciolfi, F. Cipressa, I. Moroni, V. Leuzzi, L. Pieroni, F. Marini, O. Boespflug Tanguy, E. Eymard-Pierre, F. R. Danti, C. Compagnucci, G. Zambruno, A. Brusco, F. M. Santorelli, L. Chiapparini, P. Francalanci, A. L. Loizzo, M. Tartaglia, G. Cestra, E. Bertini, Biallelic mutations in RNF220 cause laminopathies featuring leukodystrophy, ataxia and deafness. *Brain* **144**, 3020–3035 (2021).
32. H. Guo, J. M. Christoff, V. E. Campos, X. L. Jin, Y. Li, Normal corpus callosum in Emx1 mutant mice with C57BL/6 background. *Biochem. Biophys. Res. Commun.* **276**, 649–653 (2000).
33. Q. Kong, W. Zeng, J. Wu, W. Hu, C. Li, B. Mao, RNF220, an E3 ubiquitin ligase that targets Sin3B for ubiquitination. *Biochem. Biophys. Res. Commun.* **393**, 708–713 (2010).
34. A. Contractor, C. Mulle, G. T. Swanson, Kainate receptors coming of age: Milestones of two decades of research. *Trends Neurosci.* **34**, 154–163 (2011).
35. W. Lu, Y. Shi, A. C. Jackson, K. Bjorgan, M. J. During, R. Sprengel, P. H. Seeburg, R. A. Nicoll, Subunit composition of synaptic AMPA receptors revealed by a single-cell genetic approach. *Neuron* **62**, 254–268 (2009).
36. M. Prieto, A. Folci, G. Poupon, S. Schiavi, V. Buzzelli, M. Pronot, U. Francois, P. Pousinha, N. Lattuada, S. Abelanet, S. Castagnola, M. Chafai, A. Khayachi, C. Gwizdek, F. Brau, E. Deval, M. Francolini, B. Bardoni, Y. Humeau, V. Trezza, S. Martin, Missense mutation of Fmr1 results in impaired AMPAR-mediated plasticity and socio-cognitive deficits in mice. *Nat. Commun.* **12**, 1557 (2021).
37. N. N. Chang, C. H. Sun, L. Gao, D. Zhu, X. F. Xu, X. J. Zhu, J. W. Xiong, J. J. Xi, Genome editing with RNA-guided Cas9 nuclease in zebrafish embryos. *Cell Res.* **23**, 465–472 (2013).
38. T. Lalanne, J. Oyrer, M. Farrant, P. J. Sjostrom, Synapse type-dependent expression of calcium-permeable AMPA receptors. *Front. Synaptic Neurosci.* **10**, 34 (2018).
39. A. M. Mabb, Historical perspective and progress on protein ubiquitination at glutamatergic synapses. *Neuropharmacology* **196**, 108690 (2021).
40. A. J. George, Y. C. Hoffiz, A. J. Charles, Y. Zhu, A. M. Mabb, A comprehensive atlas of E3 ubiquitin ligase mutations in neurological disorders. *Front. Genet.* **9**, 29 (2018).
41. C. Rodriguez, I. Sanchez-Moran, S. Alvarez, P. Tirado, D. M. Fernandez-Mayoralas, B. Calleja-Perez, A. Almeida, A. Fernandez-Jaen, A novel human Cdh1 mutation impairs anaphase promoting complex/cyclosome activity resulting in microcephaly, psychomotor retardation, and epilepsy. *J. Neurochem.* **151**, 103–115 (2019).
42. S. N. Manivannan, J. Roovers, N. Smal, C. T. Myers, D. Turkdogan, F. Roelens, O. Kanca, H. L. Chung, T. Scholz, K. Hermann, T. Bierhals, H. S. Caglayan, H. Stamberger, H. Mefford, P. de Jonghe, S. Yamamoto, S. Weckhuysen, H. J. Bellen, De novo FZR1 loss-of-function variants cause developmental and epileptic encephalopathies. *Brain* **145**, 1684–1697 (2022).
43. L. M. Dibbens, S. E. Heron, J. C. Mulley, A polygenic heterogeneity model for common epilepsies with complex genetics. *Genes Brain Behav.* **6**, 593–597 (2007).
44. A. S. Allen, S. F. Berkovic, P. Cossette, N. Delanty, D. Dlugos, E. E. Eichler, M. P. Epstein, T. Glauser, D. B. Goldstein, Y. Han, E. L. Heinzen, Y. Hitomi, K. B. Howell, M. R. Johnson, R. Kuzniecky, D. H. Lowenstein, Y. F. Lu, M. R. Madou, A. G. Marson, H. C. Mefford, S. E. Nieh, T. J. O'Brien, R. Ottman, S. Petrovski, A. Poduri, E. K. Ruzzo, I. E. Scheffer, E. H. Sherr, C. J. Yuskaitis, B. Abou-Khalil, B. K. Alldredge, J. F. Bautista, A. Boro,

G. D. Cascino, D. Consalvo, P. Crumrine, O. Devinsky, M. Fiol, N. B. Fountain, J. French, D. Friedman, E. B. Geller, S. Glynn, S. R. Haut, J. Hayward, S. L. Helmers, S. Joshi, A. Kanner, H. E. Kirsch, R. C. Knowlton, E. H. Kossoff, R. Kuperman, S. M. McGuire, P. V. Motika, E. J. Novotny, J. M. Paolicchi, J. M. Parent, K. Park, R. A. Shellhaas, J. J. Shih, R. Singh, J. Sirven, M. C. Smith, J. Sullivan, L. L. Thio, A. Venkat, E. P. Vining, G. K. Von Allmen, J. L. Weisenberg, P. Widdess-Walsh, M. R. Winawer, De novo mutations in epileptic encephalopathies. *Nature* **501**, 217–221 (2013).

45. L. Broix, H. Jagline, E. Ivanova, S. Schmucker, N. Drouot, J. Clayton-Smith, A. T. Pagnamenta, K. A. Metcalfe, B. Isidor, U. W. Louvier, A. Poduri, J. C. Taylor, P. Tilly, K. Poirier, Y. Saillour, N. Lebrun, T. Stemmelen, G. Rudolf, G. Muraca, B. Saintpierre, A. Elmorjani, M. Moise, N. B. Weirauch, R. Guerrini, A. Boland, R. Olaso, C. Masson, R. Tripathy, D. Keays, C. Beldjord, L. Nguyen, J. Godin, U. Kini, P. Nischke, J. F. Deleuze, N. Bahi-Buisson, I. Sumara, M. V. Hinckelmann, J. Chelly, Mutations in the HECT domain of NEDD4L lead to AKT-mTOR pathway deregulation and cause periventricular nodular heterotopia. *Nat. Genet.* **48**, 1349–1358 (2016).
46. K. Kato, F. Miya, I. Hori, D. Ieda, K. Ohashi, Y. Negishi, A. Hattori, N. Okamoto, M. Kato, T. Tsunoda, M. Yamasaki, Y. Kanemura, K. Kosaki, S. Saitoh, A novel missense mutation in the HECT domain of NEDD4L identified in a girl with periventricular nodular heterotopia, polymicrogyria and cleft palate. *J. Hum. Genet.* **62**, 861–863 (2017).
47. K. Stouffs, P. Verloo, S. Brock, L. Regal, D. Beysen, B. Ceulemans, A. C. Jansen, M. E. C. Meuwissen, Recurrent NEDD4L variant in periventricular nodular heterotopia, polymicrogyria and syndactyly. *Front. Genet.* **11**, 26 (2020).
48. S. Vicari, F. Costanzo, D. Menghini, Memory and learning in intellectual disability. *Int. Rev. Res. Dev. Disabil.* **50**, 119–148 (2016).
49. M. Alemany-Gonzalez, T. Gener, P. Nebot, M. Vilademunt, M. Dierssen, M. V. Puig, Prefrontal-hippocampal functional connectivity encodes recognition memory and is impaired in intellectual disability. *Proc. Natl. Acad. Sci. U.S.A.* **117**, 11788–11798 (2020).
50. L. Zhang, N. N. Song, Q. Zhang, W. Y. Mei, C. H. He, P. Ma, Y. Huang, J. Y. Chen, B. Mao, B. Lang, Y. Q. Ding, Satb2 is required for the regionalization of retrosplenial cortex. *Cell Death Differ.* **27**, 1604–1617 (2020).
51. F. Zeng, X. Ma, L. Zhu, Q. Xu, Y. Zeng, Y. Gao, G. Li, T. Guo, H. Zhang, X. Tang, Z. Wang, Z. Ye, L. Zheng, Q. Zheng, K. Li, J. Lu, X. Qi, H. Luo, X. Zhang, Y. Zhou, Y. Yao, R. Ke, Y. Liu, H. Sun, T. Huang, Z. Shao, H. Xu, X. Wang, The deubiquitinase USP6 affects memory and synaptic plasticity through modulating NMDA receptor stability. *PLOS Biol.* **17**, e3000525 (2019).
52. N. Sheng, M. A. Bemben, J. Diaz-Alonso, W. Tao, Y. S. Shi, R. A. Nicoll, LTP requires postsynaptic PDZ-domain interactions with glutamate receptor/auxiliary protein complexes. *Proc. Natl. Acad. Sci. U.S.A.* **115**, 3948–3953 (2018).
53. Y. Zhou, T. Kaiser, P. Monteiro, X. Zhang, M. S. Van der Goes, D. Wang, B. Barak, M. Zeng, C. Li, C. Lu, M. Wells, A. Amaya, S. Nguyen, M. Lewis, N. Sanjana, M. Zhang, F. Zhang, Z. Fu, G. Feng, Mice with Shank3 mutations associated with ASD and schizophrenia display both shared and distinct defects. *Neuron* **89**, 147–162 (2016).
54. J. X. Dai, H. L. Han, M. Tian, J. Cao, J. B. Xiu, N. N. Song, Y. Huang, T. L. Xu, Y. Q. Ding, L. Xu, Enhanced contextual fear memory in central serotonin-deficient mice. *Proc. Natl. Acad. Sci. U.S.A.* **105**, 11981–11986 (2008).

Acknowledgments: We are grateful to all members of the Sheng, Mao, and Ding laboratories for discussion of and comments on the manuscript. We would like to thank the Core Technology Facility of Kunming Institute of Zoology (KIZ), Chinese Academy of Sciences (CAS) for providing us with core facility for brain functional connection study and FV1000 confocal microscope and the Service Center for Bioactivity Screening of Kunming Institute of Botany (KIB), CAS for providing us with Leica SP8 confocal microscope and CryoStar NX50 freezing microtome. **Funding:** This work was supported by grants from the Strategic Priority Research Program of the Chinese Academy of Sciences (XDPB17), National Natural Science Foundation of China (31871032, 31871483, and 32170965), the Chinese Academy of Sciences Pioneer Hundred Talents Program (to N.S.), Yunnan Fundamental Research Projects (2019FA008, 2019FJ003, 202105AC160161, 202101AW070044, and 202001AS070036), CAS "Light of West China" Program (xbzg-zdsys-201913), Shanghai Municipal Science and Technology Major Project (2018SHZDZX01), Zhangjiang (ZJ) Lab, and Shanghai Center for Brain Science and Brain-Inspired Technology. P.M. was supported by the Youth Innovation Promotion Association of Chinese Academy of Sciences. **Author contributions:** N.S., B.M., and Y.-Q.D. designed the experiments. P.M., L.P.W., Y.L., C.-H.H., N.-N.S., S.Z., and H.W. performed the experiments. P.M., L.P.W., Y.L., and C.-H.H. analyzed data. N.S., P.M., and L.P.W. wrote the paper. **Competing interests:** The authors declare that they have no competing interests. **Data and materials availability:** All data needed to evaluate the conclusions in the paper are present in the paper and/or the Supplementary Materials.

Submitted 11 April 2022
Accepted 15 August 2022
Published 30 September 2022
10.1126/sciadv.abq4736